ARTICLE

STRIPAK regulates Slik localization to control mitotic morphogenesis and epithelial integrity

Camille Valérie De Jamblinne[1,4], Barbara Decelle[1], Mehrnoush Dehghani[2,3], Mathieu Joseph[2,4], Neera Sriskandarajah[2,3], Kévin Leguay[1,4], Basile Rambaud[1,4], Sébastien Lemieux[1,5], Philippe P. Roux[1,4,6], David R. Hipfner[2,3,4,7], and Sébastien Carréno[1,4,6]

Proteins of the ezrin, radixin, and moesin (ERM) family control cell and tissue morphogenesis. We previously reported that moesin, the only ERM in *Drosophila*, controls mitotic morphogenesis and epithelial integrity. We also found that the Pp1-87B phosphatase dephosphorylates moesin, counteracting its activation by the Ste20-like kinase Slik. To understand how this signaling pathway is itself regulated, we conducted a genome-wide RNAi screen, looking for new regulators of moesin activity. We identified that Slik is a new member of the striatin-interacting phosphatase and kinase complex (STRIPAK). We discovered that the phosphatase activity of STRIPAK reduces Slik phosphorylation to promote its cortical association and proper activation of moesin. Consistent with this finding, inhibition of STRIPAK phosphatase activity causes cell morphology defects in mitosis and impairs epithelial tissue integrity. Our results implicate the Slik–STRIPAK complex in the control of multiple morphogenetic processes.

Introduction

Cell morphogenesis is an important process by which cells adapt their shapes to achieve different functions. Filaments of the actin and microtubule cytoskeletons play important roles during this process. Actin filaments apply forces to the cortex to contribute to plasma membrane remodeling, whereas microtubules are important for targeted trafficking and signaling (Koenderink and Paluch, 2018; Stephens, 2012). Proteins of the ezrin, radixin, and moesin (ERM) family link actin filaments and microtubules to the plasma membrane (Solinet et al., 2013). They regulate important cellular processes, such as cell division, migration, and epithelial organization (Fehon et al., 2010). The phosphorylation of a conserved threonine residue in the C-terminus of ERMs promotes their activation. ERMs cycle between an active conformation at the plasma membrane and an inactive form in the cytosol. An intramolecular interaction between the N-terminal FERM domain and C-terminal tail (C-terminal ERM association domain [CERMAD]) inactivates ERMs. Their activation involves a conformational switch through a multistep mechanism: (1) Phosphatidylinositol 4, 5-bisphosphate (PtdIns(4,5)P$_2$), a phospholipid of the plasma membrane, recruits ERMs to the cortex and slightly opens the molecules; (2) this preopening allows access to LOK, a sterile 20 (Ste20)-like Ser/Thr protein kinase that wedges between the FERM and CERMAD domains to complete full ERM opening; and (3) the kinase phosphorylates the regulatory

threonine of ERMs to stabilize their open conformation. This opening unmasks the actin-binding site in the CERMAD and the microtubule-interacting site in the FERM domain and allows ERMs to link actin and microtubule filaments at the plasma membrane to regulate cell morphogenesis.

Our laboratories have studied the function and regulation of moesin, the only ERM orthologue in *Drosophila melanogaster* (Polesello and Payre, 2004). We found that moesin controls epithelial integrity and mitotic morphogenesis (Carreno et al., 2008; Hipfner et al., 2004; Panneton et al., 2015; Roubinet et al., 2011; Solinet et al., 2013). In *Drosophila* wing imaginal discs, we discovered that Slik, the *Drosophila* orthologue of mammalian SLK and LOK, phosphorylates moesin to control epithelial tissue integrity. Cells lacking either Slik or moesin undergo an epithelial-to-mesenchymal transition (EMT), sort basally out of the wing disc epithelium, and undergo apoptosis (Hipfner et al., 2004; Nakajima et al., 2013; Speck et al., 2003).

In *Drosophila* S2 cells in culture, we showed that moesin controls mitotic cell shape and organization of the mitotic spindle. We found that mitosis entry is characterized by an approximately threefold increase in moesin phosphorylation. We found that Slik is responsible for the basal level of moesin phosphorylation in interphase and for the specific activation of moesin in mitosis (Carreno et al., 2008). In metaphase,

[1]Institute for Research in Immunology and Cancer, Université de Montréal, Montréal, Quebec, Canada; [2]Institut de recherches cliniques de Montréal, Montréal, Quebec, Canada; [3]Division of Experimental Medicine, McGill University, Montreal, Quebec, Canada; [4]Programmes de biologie moléculaire, Université de Montréal, Montréal, Quebec, Canada; [5]Département de Biochimie, Université de Montréal, Montréal, Quebec, Canada; [6]Département de Pathologie et de Biologie Cellulaire, Université de Montréal, Montréal, Quebec, Canada; [7]Département de Médecine, Université de Montréal, Montréal, Quebec, Canada.

Correspondence to David R. Hipfner: david.hipfner@ircm.qc.ca; Sébastien Carréno: sebastien.carreno@umontreal.ca.

phosphorylated moesin (p-moesin) spreads around the cortex and increases global cortical rigidity by coupling actin forces to the plasma membrane (Carreno et al., 2008; Kunda et al., 2008). This promotes rounding of cells. In addition, moesin–microtubule interactions regulate mitotic spindle organization (Solinet et al., 2013). In anaphase, the Ser/Thr phosphatase Pp1-87B dephosphorylates moesin at the poles and favors p-moesin accumulation at the equator (Kunda et al., 2012; Roubinet et al., 2011). This redistribution drives cell elongation and cytokinesis. After abscission, Pp1-87B dephosphorylates moesin to allow cortex relaxation (Roubinet et al., 2011). Either inhibition or overactivation of moesin has damaging effects in mitosis. Overactivation of moesin overstiffens the polar cortex in anaphase, preventing cell elongation and cytokinesis (Roubinet et al., 2011). Conversely, moesin or Slik double-stranded RNA (dsRNA) depletion renders the cortex too soft; cells do not control mitotic morphogenesis properly and present abnormal cortical blebs (Carreno et al., 2008).

In addition to Pp1-87B and Slik, we also found that the PtdIns-4-kinase CG10260 and the PtdIns(4)P 5-kinase Skittles regulate localized PtdIns(4,5)P_2 production at the plasma membrane to control moesin localization (Roch et al., 2010; Roubinet et al., 2011; Tan et al., 2014). However, we still do not know how the enzymes of the signaling network activating moesin are themselves regulated. To this end, we performed an unbiased genome-wide dsRNA screen in *Drosophila* S2 cells and measured p-moesin levels. We found that the striatin-interacting phosphatase and kinase complex (STRIPAK) is a positive regulator of moesin phosphorylation. At the core of the STRIPAK complex, there is a protein Ser/Thr phosphatase 2A (hereafter referred to as "PP2A$_{STRIPAK}$"; Fig. 1 A; Goudreault et al., 2009; Hwang and Pallas, 2014). PP2A$_{STRIPAK}$ is a heterotrimeric enzyme that consists of a PP2A catalytic C subunit (Mts, in *Drosophila*), a PP2A scaffold A subunit (PP2A-29B), and a striatin regulatory B subunit (Cka). On top of this core, striatin-interacting proteins known as STRIPs (Strip) help to scaffold Ser/Thr kinases of the Ste20-like family (Ashton-Beaucage et al., 2014; Goudreault et al., 2009; Madsen et al., 2015; Ribeiro et al., 2010; Tang et al., 2019).

STRIPAK controls the activity of its associated kinases, either by regulating phosphorylation of regulatory residues (Gordon et al., 2011; Zheng et al., 2017) or by recruiting them to specific sites in the cell (Kean et al., 2011). Thereby, STRIPAK affects cell proliferation and survival, cytoskeletal regulation, and vesicle trafficking (Kück et al., 2019). Here, we show that Slik is a new STRIPAK-associated kinase. We found that PP2A$_{STRIPAK}$ promotes Slik association with the cortex by regulating its phosphorylation status. Finally, we show that PP2A$_{STRIPAK}$ controls Slik and moesin functions to regulate mitotic morphogenesis and epithelial integrity. Our results place STRIPAK as a critical upstream regulator of cell morphogenesis through its effects on Slik and, ultimately, moesin.

Results

A genome-wide RNAi screen identifies *Drosophila* STRIPAK (dSTRIPAK) as an activator of moesin

To identify activators of Slik and moesin, we performed a genome-wide screen using an RNAi library covering 90% of the *Drosophila* genome. We screened for genes whose depletion triggers a decrease of moesin phosphorylation in *Drosophila* S2 cells. To this aim, we developed an immunofluorescence high-content screening method using an antibody specific to phosphorylated Thr559 moesin (Carreno et al., 2008). We initially identified 201 genes acting as potential moesin activators (Fig. 1 B). Among these genes, we found *moesin* itself and all previously characterized positive regulators (*slik, skittles,* and *CG10260*; Carreno et al., 2008; Hipfner et al., 2004; Roubinet et al., 2011; Tan et al., 2014), confirming the specificity and sensitivity of our screening procedure. Of the 201 genes found, we validated 51 genes in a secondary screen using alternative nonoverlapping dsRNAs (Fig. 1 C and Table S1). Among these moesin activators, we investigated the function of a set of genes associated with the dSTRIPAK complex (Ribeiro et al., 2010): connector of kinase to AP-1 (Cka), Strip, and PP2A scaffolding subunit (PP2A-29B).

dSTRIPAK phosphatase activity regulates moesin phosphorylation

STRIPAK is an evolutionarily conserved multiprotein complex that functionally links the phosphatase activity of PP2A to different Ste20-like kinases (Gordon et al., 2011; Goudreault et al., 2009; Kim et al., 2020; Kück et al., 2019; Ribeiro et al., 2010; Shi et al., 2016). Both enzymatic functions are scaffolded by striatin proteins (Fig. 1 A). Striatins also function as the STRIPAK-specific PP2A regulatory subunits (B‴) and control PP2A$_{STRIPAK}$ subcellular localization and substrate specificity (Janssens and Goris, 2001; Kück et al., 2019; Moreno et al., 2001). Cka, the only *Drosophila* striatin, interacts with Strip and is considered as a constituent of PP2A$_{STRIPAK}$ (Ashton-Beaucage et al., 2014), although its function is not totally understood. Finally, proteins of the striatin family interact either directly or indirectly through adapter proteins with Ste20-like kinases from different germinal center kinase (GCK) subfamilies (Hwang and Pallas, 2014; Kyriakis, 1999; Shi et al., 2016).

The components of dSTRIPAK that were identified as moesin activators are all members of PP2A$_{STRIPAK}$ (Fig. 1 A). We did not identify any of the adapter proteins or the three kinases known to associate with dSTRIPAK. We performed the primary round of the genome-wide screen using a single dsRNA per gene, opening the possibility of false-negative results. We therefore decided to test the implication of the other dSTRIPAK members in moesin regulation by using additional nonoverlapping dsRNAs. Because moesin displays an approximately threefold increase of phosphorylation at mitotic entry (Carreno et al., 2008; Roubinet et al., 2011), we also investigated if members of dSTRIPAK regulate moesin specifically in interphase and/or mitosis. After dsRNA knockdown, we colabeled p-moesin and p-histone H3, a marker of mitotic cells, and quantified the levels of p-moesin in interphase and mitosis. This experiment revealed that the depletion of Mob4, Slmap, and FGOP2, three different dSTRIPAK adapter proteins, slightly decrease p-moesin levels (Fig. S1 A).

Because kinases play important roles in STRIPAK functions, we investigated the role of the three known dSTRIPAK-associated kinases on moesin phosphorylation. Even if we cannot rule out that the additional dsRNAs targeting GckIII,
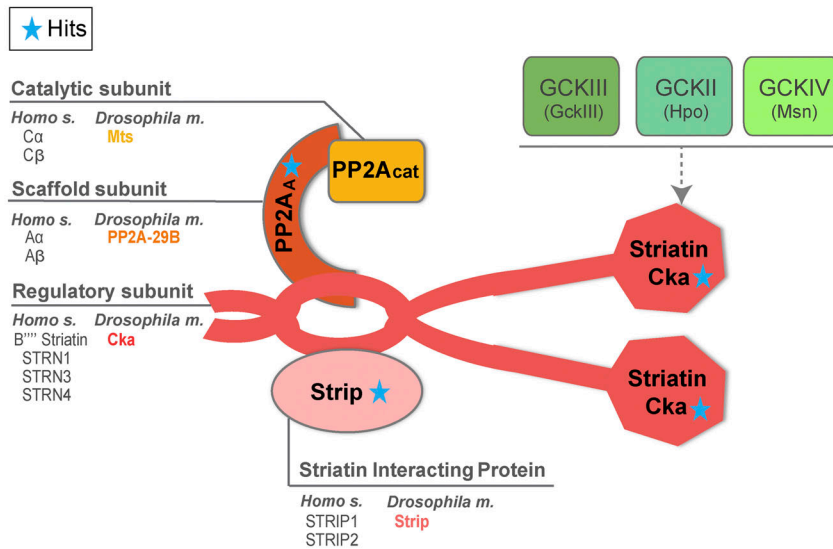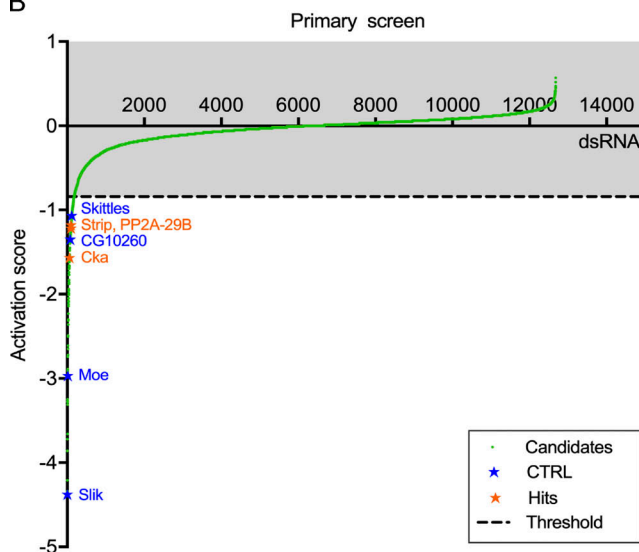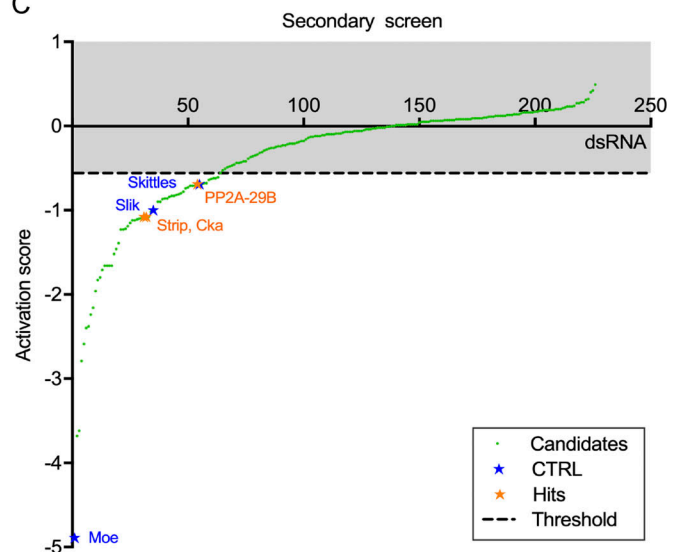
Figure 1. **A genome-wide RNAi screen identifies the dSTRIPAK complex as a moesin activator. (A)** Representation of the dSTRIPAK complex with members controlling moesin phosphorylation identified in screen are highlighted with a blue star. **(B and C)** The activation score was calculated for each dsRNA on the basis of mean intensity of p-moesin and ranked by increasing score for the primary RNAi screen (B) and secondary confirmation screen (C). Genes known to control moesin phosphorylation are shown with blue stars, and genes of dSTRIPAK are shown with orange stars. Thresholds are marked by dashed lines (see Materials and methods). CTRL, control; *Drosophila m., Drosophila melanogaster; Homo s., Homo sapiens*; Moe, moesin; PP2Acat, PP2A catalytic subunit.

Hpo, and Msn did not efficiently knock down these kinases, none of these dsRNAs affected p-moesin levels (Fig. 2 A). In accordance with our primary screen, we also found that single knockdown of Cka, Strip, and PP2A-29B with two independent dsRNAs triggers a significant decrease of p-moesin in both interphase and mitosis (Fig. 2 A). In addition to these three PP2A$_{STRIPAK}$ members, we found that dsRNA depletion of Mts, the catalytic subunit of PP2A$_{STRIPAK}$, decreased the levels of p-moesin. We did not originally identify Mts as a moesin activator in the primary screen, but we found that the dsRNA of the RNAi library targeting Mts did not fully deplete the protein (Fig. S1, B and C; dsRNA Mts-1). Interestingly, we also found that Cka depletion reduces Strip protein levels without

affecting its mRNA levels (Fig. S1, D–F). This suggests that through their interaction, Cka stabilizes Strip.

The identification of each member of PP2A$_{STRIPAK}$ as a moesin activator suggests that dSTRIPAK phosphatase activity regulates moesin. To confirm this, we used okadaic acid (OA), a phosphatase inhibitor that specifically inhibits PP2A at low concentrations (<1 μM) while inhibiting both PP2A and PP1 at higher concentrations (Cohen et al., 1989; Favre et al., 1997). Upon OA treatment at low concentration to solely inhibit PP2A, we observed a significant reduction of p-moesin by Western blotting (Fig. 2, B and C). Because the catalytic (Mts) and structural (PP2A-29B) subunits of PP2A are shared by the different PP2A holoenzymes (Janssens et al., 2005), we tested the !
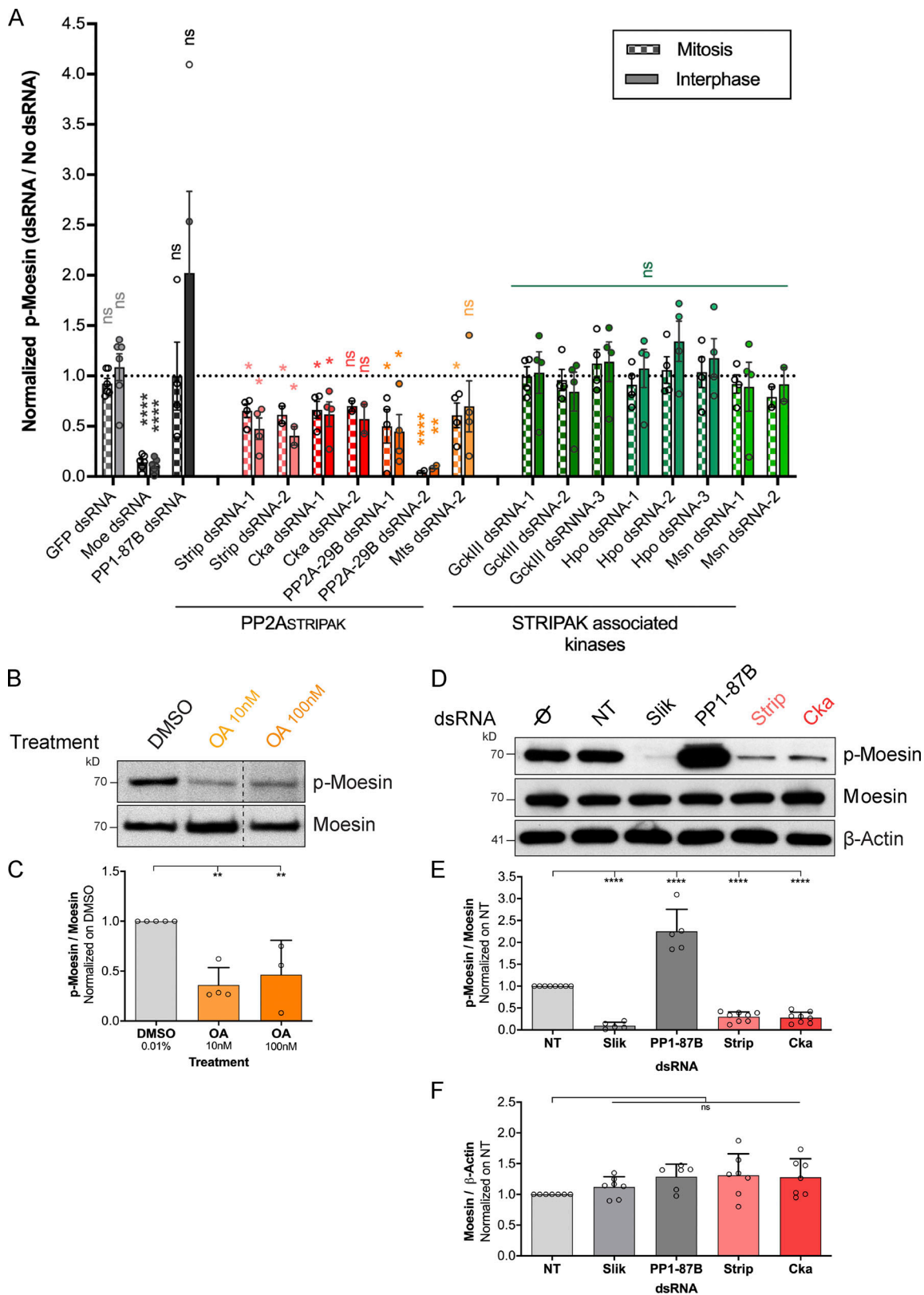
Figure 2. **dSTRIPAK phosphatase activity regulates moesin phosphorylation. (A)** p-Moesin immunofluorescence intensity in S2 cells treated as indicated and normalized to the nontreated condition. Data are represented as normalized mean ± SEM of two to four independent experiments (circles), and two-tailed unpaired *t* tests were calculated against the nontreated condition. **(B and D)** Western blot of S2 cells treated as indicated. **(C, E, and F)** Relative p-moesin levels and relative moesin levels normalized as indicated in three to eight independent experiments (circles). Data are represented as normalized mean ± SD, one-way ANOVA with the following P values: NS, P > 0.05; *, P < 0.05; **, P < 0.01; ****, P < 0.0001.

four other PP2A regulatory B subunits using validated dsRNAs (Chen et al., 2007). We found that well-rounded (Wrd), B″, and widerborst (Wdb) dsRNA depletion did not affect moesin phosphorylation (Fig. S1, G and H). We also found that although Cka dsRNA depletion reduced p-moesin levels by ~75%, Twins (Tws) dsRNA depletion reduced p-moesin levels by almost 50% (Fig. S1, G and H). The function of PP2A-Tws on moesin phosphorylation could be a secondary effect of its major role in mitosis (Chen et al., 2007; Mehsen et al., 2018). We thus chose to further study the function of PP2A$_{STRIPAK}$ specifically by depleting Cka or its interacting partner Strip (Gordon et al., 2011; Ribeiro et al., 2010). We confirmed that dsRNA depletion of Cka or Strip reduced p-moesin significantly without affecting overall moesin levels (Fig. 2, D–F). Taken together, our results reveal that dSTRIPAK phosphatase activity is needed for moesin activation at a post-translational level.

PP2A$_{STRIPAK}$ interacts with Slik and regulates its phosphorylation state

Most of the known functions of STRIPAK involve a functional crosstalk between PP2A$_{STRIPAK}$ and kinases that belong to the GCK family (Gordon et al., 2011; Hyodo et al., 2012; Zheng et al., 2017). However, we did not identify any of the known STRIPAK-associated kinases as moesin regulators (Fig. 2 A). Instead, we found that Slik, which is part of the GCK-V subfamily, is a new kinase associated with the dSTRIPAK complex. We expressed tagged versions of Slik together with Cka or Strip and performed reciprocal coimmunoprecipitation experiments, and we found that Stag-tagged Cka or Strip associated with GFP-tagged Slik, while they did not associate with GFP (Fig. 3, A and B).

We next wondered if Slik itself could be a target of PP2A$_{STRIPAK}$. We noticed that when proteins from S2 cells were separated on a low-percentage SDS-PAGE gel in the presence of phosphatase inhibitors, Slik appeared as two doublet bands. These bands may correspond to different Slik splicing variants. Indeed, mRNAs encoding for three Slik short isoforms (147.5, 152.1, and 155.1 kD; hereafter named "Slik-short") and mRNAs encoding for two long isoforms (184.6 and 192.1 kD; hereafter named "Slik-long") were previously identified (Fig. S2 A; http://flybase.org/reports/FBgn0035001). Consistent with this hypothesis, both doublet bands disappeared upon knockdown of all Slik isoforms, and only the upper doublet disappeared when using a dsRNA targeting Slik-long specifically (Fig. S2, B and C). Upon λ-phosphatase treatment, we found that both Slik-long and Slik-short doublets disappeared to migrate both as unique bands with increased mobility, demonstrating that Slik is phosphorylated (Fig. 3, C and D). Thus, we can detect Slik phosphorylation by apparent mobility shift. Importantly, we found that PP2A$_{STRIPAK}$ regulates Slik phosphorylation because inhibition of PP2A enzymatic activity using OA, or knockdown of individual members of PP2A$_{STRIPAK}$, promoted a greater mobility shift of Slik-long and Slik-short than in control conditions (Fig. 3, E–G). These mobility shifts were abolished upon λ-phosphatase treatment, further demonstrating that the retarded bands correspond to phosphorylated forms of Slik (Fig. S2, D and E).

PP2A$_{STRIPAK}$ regulates Slik localization at the cell cortex

We then asked if PP2A$_{STRIPAK}$ could regulate Slik function. We found that PP2A$_{STRIPAK}$ does not regulate the stability or the catalytic activity of Slik. First, Strip or Cka dsRNA depletion did not affect the stability of either the Slik-long or Slik-short isoform (Fig. S2, F and G). Next, we immunoprecipitated endogenous Slik and measured its kinase activity in vitro on its natural substrate, the C-terminal part of moesin (Plutoni et al., 2019). We found that the depletion of Strip, Cka, PP2A-29B, or Mts did not affect the kinase activity of Slik (Fig. S2, H and I).

STRIPAK can regulate the function of Ste20-like kinases by controlling their localization (Elramli et al., 2019; Kean et al., 2011; Zheng et al., 2017). We thus tested if PP2A$_{STRIPAK}$ regulates Slik subcellular localization. We previously reported that Slik associates with the cortex of S2 cells and epithelial cells in wing discs (Carreno et al., 2008; Hipfner et al., 2004; Roubinet et al., 2011). We measured an ~30% loss of Slik at the cortex upon Strip or Cka depletion when compared with control cells (Fig. 4, A and B; and Fig. S3 A). To test if PP2A$_{STRIPAK}$ controls Slik cortical association by regulating its phosphorylation state, we treated cells with OA to increase Slik phosphorylation levels (Fig. 3 E). We observed that Slik association with the cortex was decreased upon OA treatment (Fig. 4, C and D; and Fig. S3 B). We then used staurosporine (Stau), a broad kinase inhibitor, to block Slik phosphorylation. We observed that upon Stau treatment, Slik localization at the cortex increased significantly (Fig. 4, C and D; and Fig. S3 B). Altogether, these results demonstrate that PP2A$_{STRIPAK}$ controls Slik association with the cell cortex, potentially by regulating its phosphorylation.

PP2A$_{STRIPAK}$ regulates Slik localization by phosphorylation to control moesin activation

We reasoned that if PP2A$_{STRIPAK}$ dephosphorylates Slik to promote its association with the cortex, a phospho-deficient mutant of Slik should be enriched at the cortex. Also, the association with the cortex of this phospho-deficient mutant should not be reduced upon PP2A$_{STRIPAK}$ depletion. To dynamically follow the subcellular localization of relevant Slik mutants, we first tested if a GFP version of Slik (Slik-GFP) behaves as the endogenous kinase. As we previously reported, Slik-GFP localizes at the cell cortex (Fig. 5 A; Roubinet et al., 2011). We then observed live cells and assessed if drugs inhibiting Ser/Thr kinases or phosphatases affect Slik-GFP cortical association as we observed for the endogenous kinase. We found that OA treatment reduces association of Slik-GFP with the cortex, whereas Stau treatment increased this association (Fig. S3, C and D). As observed for endogenous Slik, we also found that dsRNA depletion of Cka or Strip decreased the association of Slik-GFP with the cortex (Fig. 5, A and B; and Fig. S3 E).

We previously identified 15 Ser/Thr that are phosphorylated on Slik (Panneton et al., 2015), and by curating available databases (Bodenmiller and Aebersold, 2011; Gnad et al., 2011; Hu et al., 2019), we identified six additional Ser/Thr potentially phosphorylated (Fig. 5 C). We constructed two different nonphosphorylatable Slik partial mutants by replacing the 17 potentially phosphorylated Ser/Thr of the nonconserved domain (NCD) by nonphosphorylatable Ala within Slik-GFP (Slik^{NCD*}-
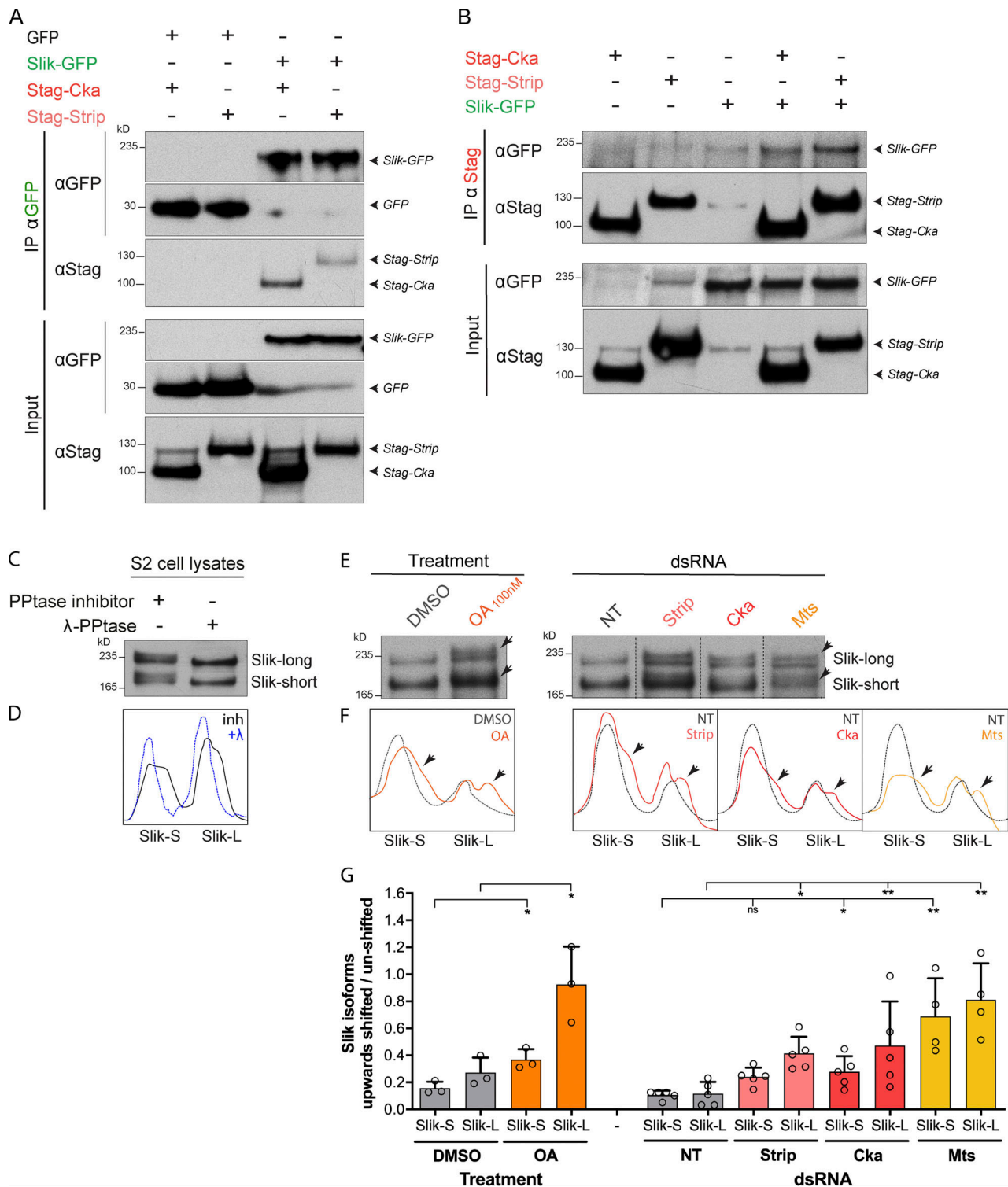
De Jamblinne et al.
STRIPAK regulates moesin functions

Journal of Cell Biology 5 of 19
https://doi.org/10.1083/jcb.201911035

Figure 3. **PP2A$_{STRIPAK}$ interacts with Slik and regulates its phosphorylation state. (A and B)** Cell lysates of S2 cells transiently expressing the indicated cDNA were immunoprecipitated (IP) with anti-GFP (A) or anti-Stag (B) antibodies and analyzed by Western blotting. **(C and E)** Western blot of S2 cells treated as indicated. **(D and F)** Line scans of C and E. Arrows indicate Slik-long (Slik-L) or Slik-short (Slik-S). **(G)** Proportion of phosphorylated Slik (upward shifted/unshifted). Data are represented as mean ± SD of three to five independent experiments (circles). Unpaired t test for drug treatments and one-way ANOVA for dsRNA conditions with the following P values: NS, $P > 0.05$; *, $P < 0.05$; **, $P < 0.01$. λ-PPtase, λ-phosphatase; NT, non-target.
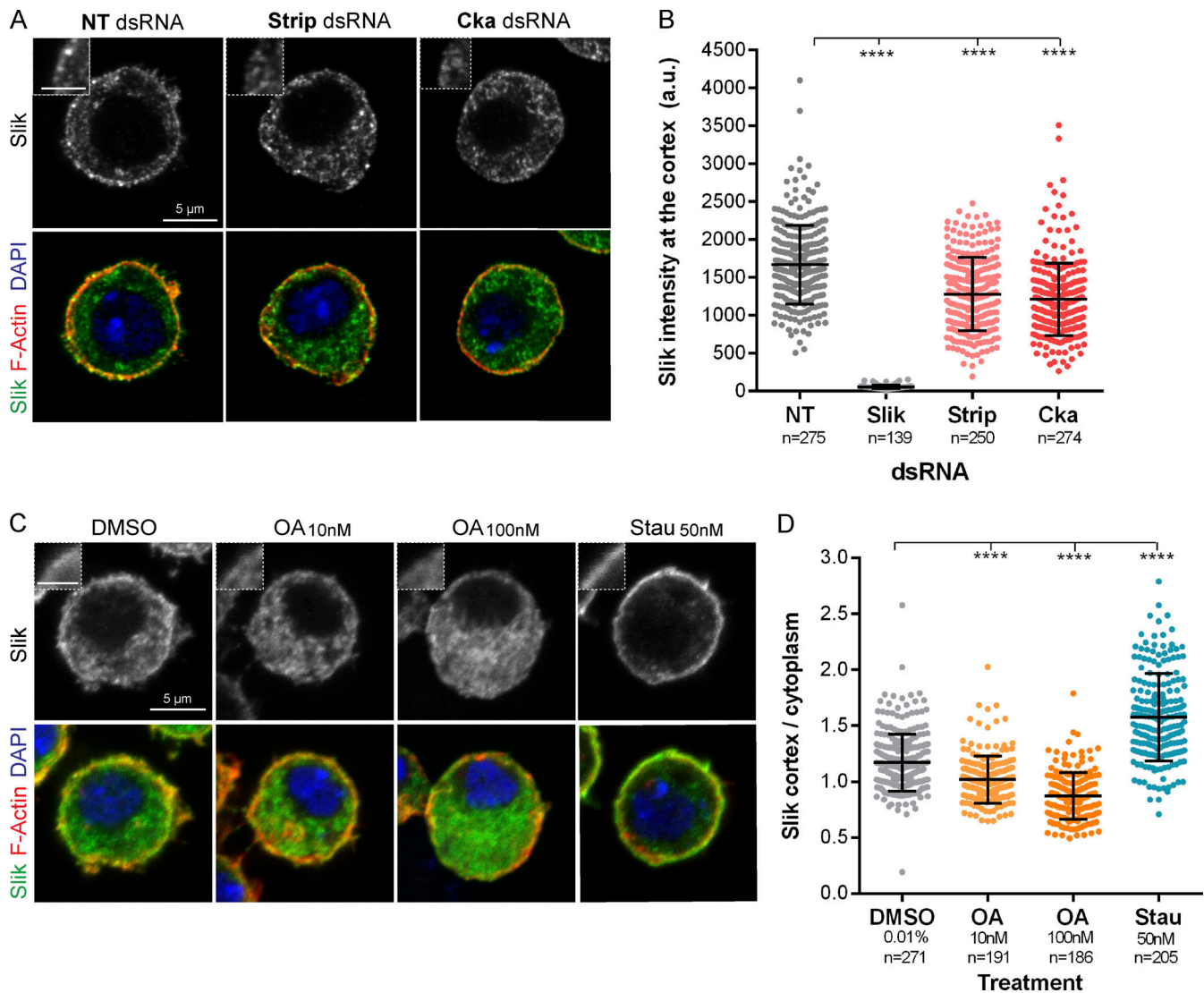
Figure 4. **PP2A$_{STRIPAK}$ regulates Slik localization at the cell cortex. (A and C)** Projection of three confocal planes of S2 cells upon the indicated treatment and stained for Slik (green), F-actin (red), and DNA (blue). Enlarged areas of the cells are shown. **(B and D)** Slik intensity at the cortex (B) or the ratio of Slik intensity (cortex/cytoplasm; D) in a minimum of 60 cells/condition in three independent experiments (see also Fig. S3). Data are represented as mean ± SD (each dot represents the value for a single cell), one-way ANOVA with the following P value: ****, P < 0.0001. Scale bars, 5 µm and 2 µm for enlarged areas.

GFP) or the 4 Ser/Thr of the C-terminal domain (CTD; Slik^{CTD*}-GFP). We found that both Slik^{NCD*}-GFP and Slik^{CTD*}-GFP were significantly enriched at the cortex when compared with Slik-GFP (Fig. 5, D and E; and Fig. S3 F). In contrast to Slik-GFP (Fig. 5, A and B), we found that Strip or Cka dsRNA depletion does not decrease the association of Slik^{NCD*}-GFP and Slik^{CTD*}-GFP with the cortex (Fig. 5 F). Finally, we showed that both Slik phospho-deficient mutants rescue or partially rescue moesin phosphorylation levels caused by PP2A$_{STRIPAK}$ depletion (Fig. 5, G and H). Although Strip or Cka dsRNA depletion reduced moesin phosphorylation in cells that stably expressed Slik-GFP, the depletion of these PP2A$_{STRIPAK}$ members only slightly affected phosphorylation of moesin in cells stably expressing similar amounts of Slik^{NCD*}-GFP or Slik^{CTD*}-GFP. These results indicate that PP2A$_{STRIPAK}$ dephosphorylates Slik to favor its association with the cortex in order to activate moesin. In addition, they suggest

that by bringing global negative charges to Slik, phosphorylation on Ser/Thr prevents the association of the kinase with the plasma membrane.

Strip and Cka control Slik cortical association in mitosis and mitotic morphogenesis

Because dSTRIPAK controls moesin phosphorylation both in interphase and in mitosis (Fig. 2 A), we next wondered if PP2A$_{STRIPAK}$ could regulate association of Slik with the cortex of mitotic cells. We followed Slik-GFP localization in live cells undergoing mitosis. We discovered that Slik becomes enriched at the cortex of control cells at the mitotic onset (Fig. 6, A and B). We then wondered if Slik cortical recruitment at mitotic entry could be affected by mutations of the potentially phosphorylated Ser/Thr we characterized above. We found that although Slik^{NCD*}-GFP and Slik^{CTD*}-GFP are both already enriched at the
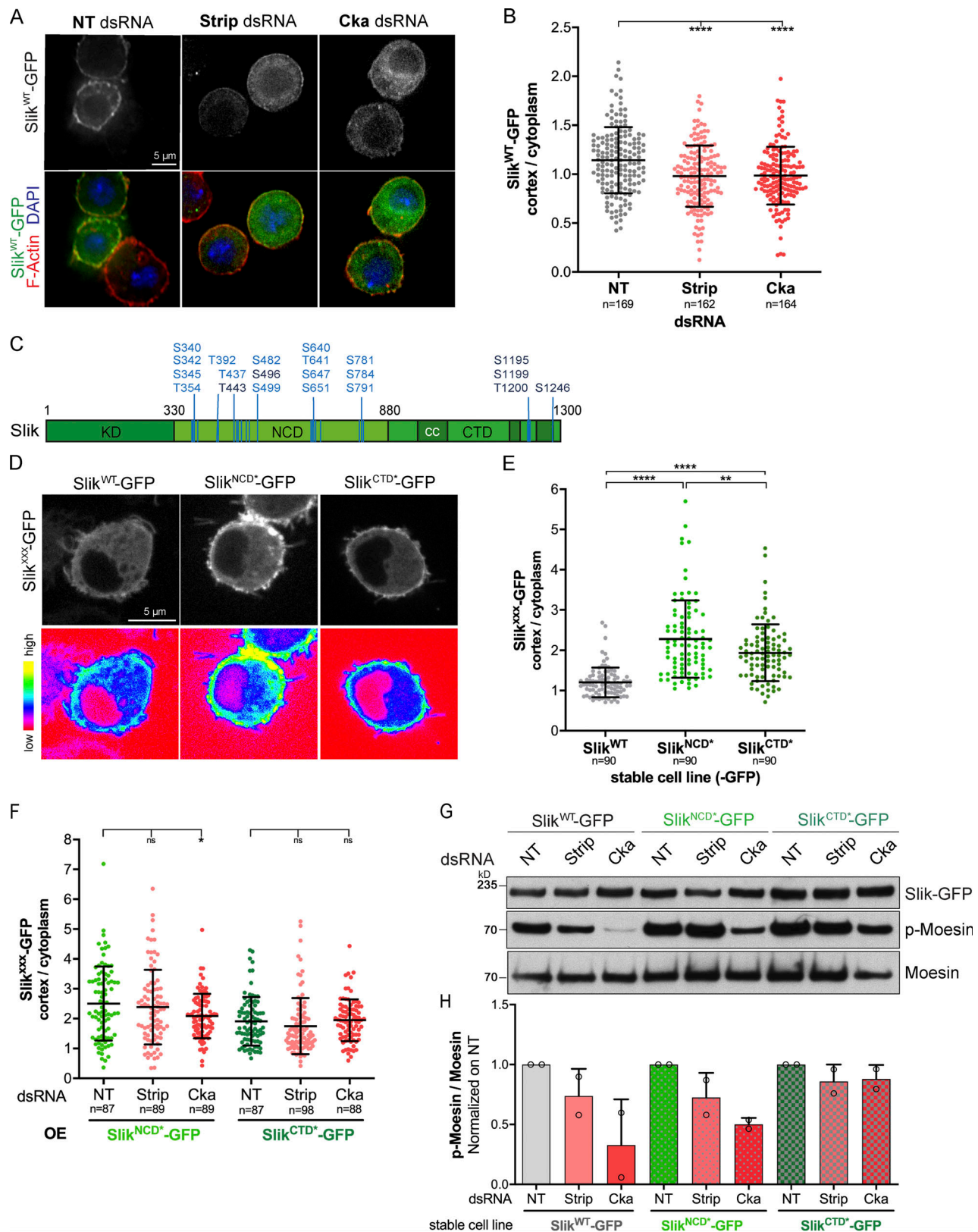
Figure 5. **PP2A$_{STRIPAK}$ regulates Slik localization by phosphorylation to control moesin activation. (A)** S2 cells stably expressing Slik^{WT}-GFP (white top row or green bottom row) upon the indicated treatment and stained for F-actin (red) and DNA (blue). **(B)** The ratio of Slik^{WT}-GFP intensity (cortex/cytoplasm) was quantified in a minimum of 40 cells/experiment in three independent experiments (see Fig. S3 D). Data are represented as mean ± SD (each dot represents the value for a single cell), one-way ANOVA. **(C)** Illustration of Slik (short isoform of 1,300 amino acids) and its kinase domain (KD), NCD, and CTD containing coiled-coil motifs (cc). Previously identified phosphosites (light blue; Panneton et al., 2015) and additional phosphosites (dark blue) are shown. **(D)** Cells

expressing the indicated Slik-GFP constructs (white top row). The signal of the indicated Slik-GFP construct was pseudocolored in a rainbow heatmap to underline variations in its localization (bottom row). **(E and F)** The ratio of Slik-GFP intensity (cortex/cytoplasm) was quantified in S2 cells stably expressing the indicated constructs. 30 (E) or 40 (F) cells/condition in three (E) or two (F) independent experiments (see Fig. S3). Data are represented as mean ± SD (each dot represents the value for a single cell), two-tailed unpaired t test (E) or one-way ANOVA (F). **(G)** Western blot of S2 cells stably expressing the indicated Slik-GFP constructs and treated as indicated. **(H)** Relative p-moesin levels (normalized to moesin) were quantified in two independent experiments (circles). Data are represented as mean ± SD normalized on nontarget (NT) dsRNA. P values are as follows: NS, $P > 0.05$; *, $P < 0.05$; **, $P < 0.01$; ****, $P < 0.0001$. Scale bars, 5 µm. OE, overexpressed.

plasma membrane in interphase when compared with Slik-GFP, they are still significantly recruited to the cortex of cells entering mitosis (Fig. 6, A and B). This suggests that other phosphorylation sites can control Slik cortical recruitment at mitotic entry. Alternatively, another underlying mechanism could control Slik recruitment to the plasma membrane of mitotic cells.

We then followed the consequences on Slik localization by inhibiting Ser/Thr phosphatases or kinases in cells undergoing mitosis. We found that, as observed in interphase, Slik is lost from the cortex upon OA treatment and enriched upon Stau treatment in metaphase (Fig. 6, C and D). Remarkably, we also discovered that impairing PP2A$_{STRIPAK}$ function through Strip or Cka dsRNA depletion partially abrogated Slik mitotic cortical recruitment (Fig. 6, E and F). This indicates that throughout the cell cycle, PP2A$_{STRIPAK}$ regulates a balance of the phosphorylation status of Slik to control the localization of the kinase at the cortex.

Having shown that PP2A$_{STRIPAK}$ regulates Slik localization and moesin activation both in interphase and in mitosis, we tested its function in mitosis. We and others previously reported that Slik and moesin are necessary to sustain mitotic cortical stability (Carreno et al., 2008; Kunda et al., 2008; Roubinet et al., 2011; Solinet et al., 2013). As we previously reported, Slik dsRNA depletion promoted cortical instability throughout each stage of mitosis, with the formation of abnormal blebs (Fig. 7, A–C). In addition, moesin is not recruited to the cortex in metaphase as a consequence of its lack of phosphorylation and activation. We observed similar, albeit milder, phenotypes upon Strip or Cka depletion (Fig. 7, A–C). Thus, as for moesin and Slik, PP2A$_{STRIPAK}$ regulates cortical stability during mitosis.

Strip and Cka control epithelial tissue integrity in *Drosophila* epithelia

Moesin plays an essential role in maintaining the integrity of epithelial tissues such as the wing imaginal disc (Speck et al., 2003). *moesin* mutant cells frequently activate expression of matrix metalloprotease 1 (Mmp1, a marker of EMT), sort basally out of the epithelium, and undergo apoptosis (Nakajima et al., 2013), leading to a broader disorganization of the disc epithelium (Speck et al., 2003). As in S2 cells, Slik is the main kinase that phosphorylates and activates moesin in the wing imaginal disc, and *slik* mutants show similar epithelial integrity defects as *moesin* mutants (Hipfner et al., 2004). We therefore tested whether epithelial integrity and moesin phosphorylation were affected by depletion of Strip and Cka in wing discs.

Evidence suggests that dSTRIPAK associates with Hippo and negatively regulates its activity in discs, promoting tissue growth. Accordingly, dsRNA-mediated depletion of Cka caused tissue undergrowth (Ribeiro et al., 2010). We used *ptc*-GAL4,

which drives transgene expression in a central stripe of cells in the wing imaginal disc (labeled by GFP expression; Fig. 8 A), to express dsRNAs targeting Strip or Cka. Strong depletion (e.g., when including a Dicer2 transgene to enhance RNAi production) of Strip or Cka was lethal. With a more moderate depletion, we observed a similar phenotype upon expression of Strip or Cka dsRNAs, with a marked reduction in the GFP-positive *ptc* domain that was most evident in cells of the prospective wing blade (or wing pouch) region of the disc (arrowheads in Fig. 8, B and C). Strip or Cka depletion was better tolerated in the more proximal wing hinge region (arrows in Fig. 8, B and C). Rather than reduced growth per se, we noticed a strong induction of apoptosis in Strip- or Cka-depleted cells, as evidenced by activated capsase-3 and pyknotic nuclei on the basal side of the *ptc* domain, mainly below the wing pouch region (Fig. 8, A–C).

Apoptosis could be a principal response to dSTRIPAK depletion or a secondary consequence of a loss of epithelial integrity as cells are extruded from the tissue. To distinguish between the two, we coexpressed the baculoviral P35 protein to inhibit apoptosis. On its own, P35 expression had little effect (Fig. 8 D). P35-expressing, Strip- or Cka-depleted cells showed improved survival. However, the rescued cells frequently activated expression of Mmp1 and sorted to the basal side of the epithelium, as seen in orthogonal projections (Fig. 8, E and F). This phenotype was similar to, though less pronounced than, that observed in P35-expressing, Slik-depleted cells (Fig. 8 G). These results suggest that apoptosis of Strip- or Cka-depleted cells is a consequence of their extrusion from the disc epithelium and are consistent with a role of dSTRIPAK in promoting epithelial tissue integrity as Slik and moesin do.

Strip and Cka control Slik localization and function in the wing disc epithelium

To test if the epithelial integrity defect triggered by Strip or Cka depletion could be linked to Slik, we used moesin phosphorylation as a specific readout of Slik activity. Because they remain viable and integrated in the epithelium, we focused on cells in the wing hinge region. Moderate depletion of Strip or Cka reduced the level of p-moesin in this region (arrows, Fig. 9, A–C). To quantify this, we measured p-moesin fluorescence intensity in GFP-positive cells in the *ptc* domain versus adjacent wild-type cells in the hinge region, where several apical–basal cross-sections of the epithelium can be seen at the folds (Fig. 9, A′–C′). In wild-type discs, p-moesin levels are uniform throughout the folds of the wing hinge region, with a small (3%) but statistically significant upregulation in cells in the *ptc* domain (Fig. 9, A′ and D). In contrast, depleting Strip (Fig. 9, B′ and E) or Cka (Fig. 9, C′ and F) caused a significant decrease in p-moesin levels (by 9% and 17%, respectively). We observed a
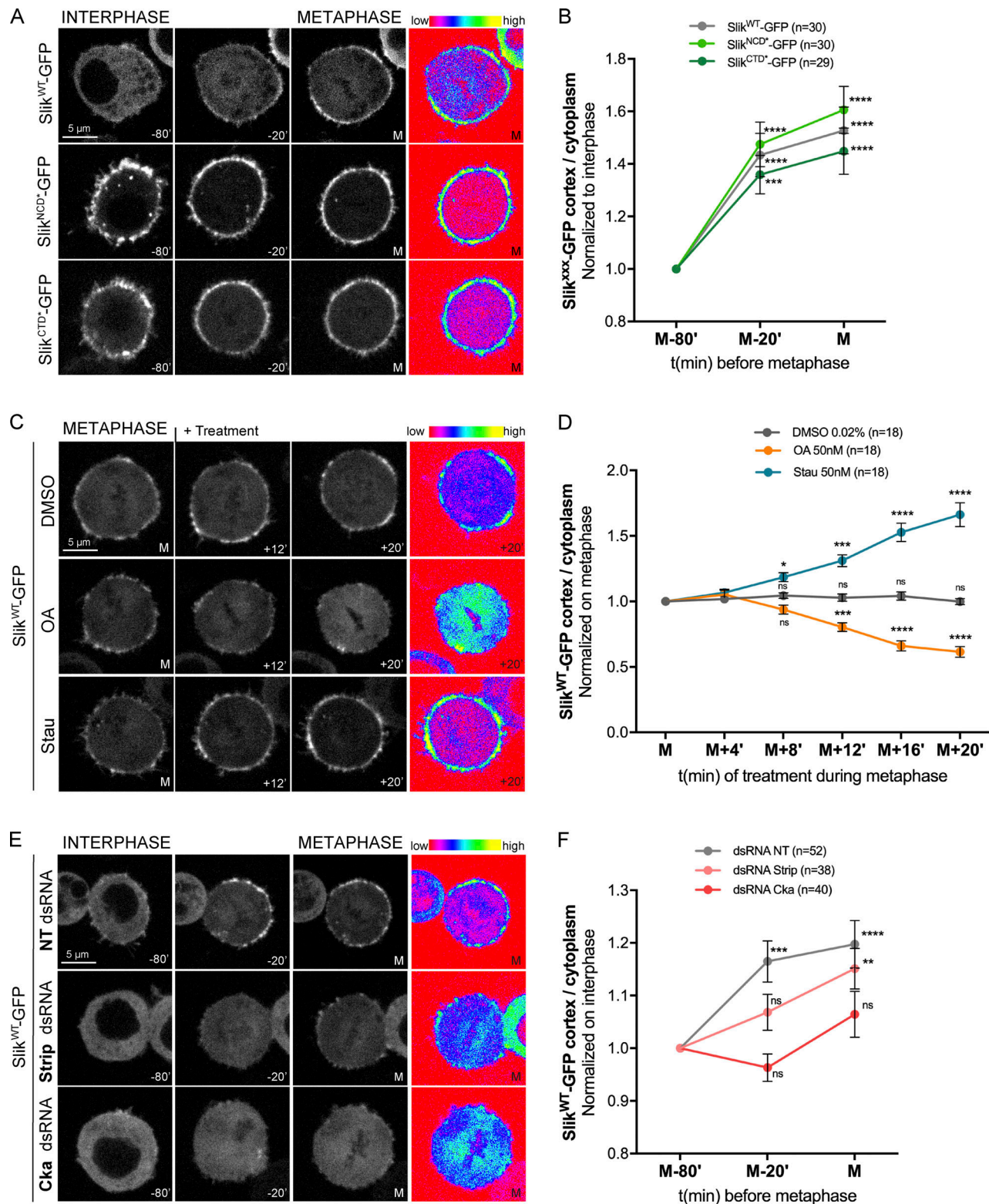
Figure 6.   **PP2A$_{STRIPAK}$ regulates Slik cortical association in mitosis. (A and E)** Time lapse of Slik distribution in live S2 cell stably expressing control or mutated Slik-GFP (white) and undergoing mitosis. Slik-GFP signals were pseudocolored in a rainbow heatmap to underline variations in its distribution in metaphase (right row). **(C)** Time lapse of Slik distribution in live S2 cell stably expressing Slik^{WT}-GFP (white) upon the indicated treatments after the first metaphase time frame. Slik^{WT}-GFP signal was pseudocolored in a rainbow heatmap to underline variations in its distribution after 20 min of treatment (right row). **(B, D, and F)** The ratios of the indicated Slik-GFP constructs (cortex/cytoplasm) were quantified and normalized to the first time frame in a minimum of six cells/condition in three independent experiments. Data are represented as normalized mean ± SEM of the pooled experiments, and one-way ANOVA was calculated against the first time frame with the following P values: NS, $P > 0.05$; *, $P < 0.05$; **, $P < 0.01$; ***, $P < 0.001$; ****, $P < 0.0001$. Scale bars, 5 µm.
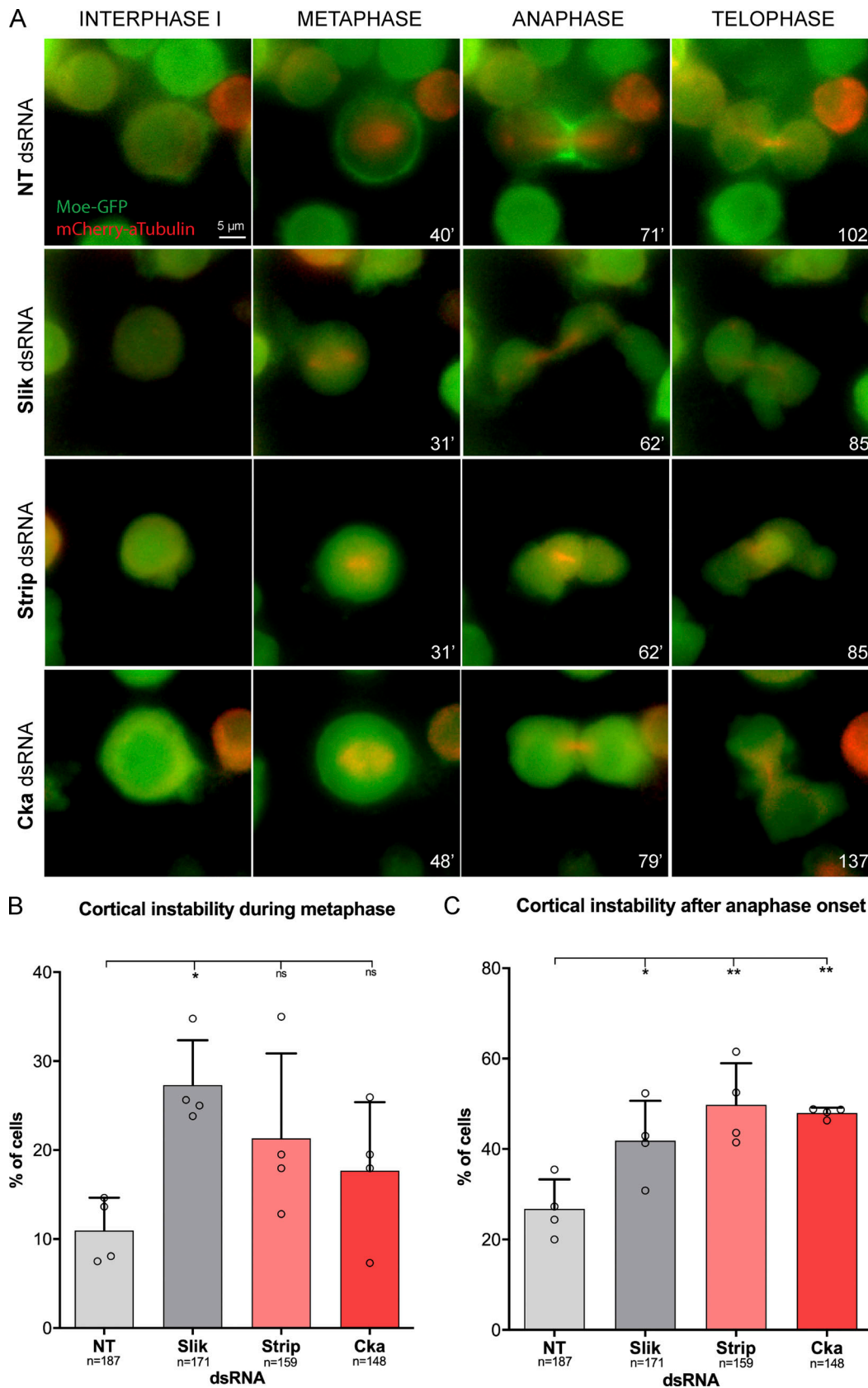
Figure 7. **Strip and Cka control mitotic morphogenesis in cultured S2 cells. (A)** Time lapse of cells stably coexpressing moesin-GFP (green) and α-tubulin-mCherry (red) treated as indicated and undergoing mitosis. **(B and C)** Percentage of cells with cortical instability in metaphase (B) or after metaphase onset (C) were quantified from live-cell recordings of four independent experiments (circles). Data are represented as mean ± SD of the pooled experiments, one-way ANOVA with the following P values: NS, $P > 0.05$; *, $P < 0.05$; **, $P < 0.01$. Scale bars, 5 µm.
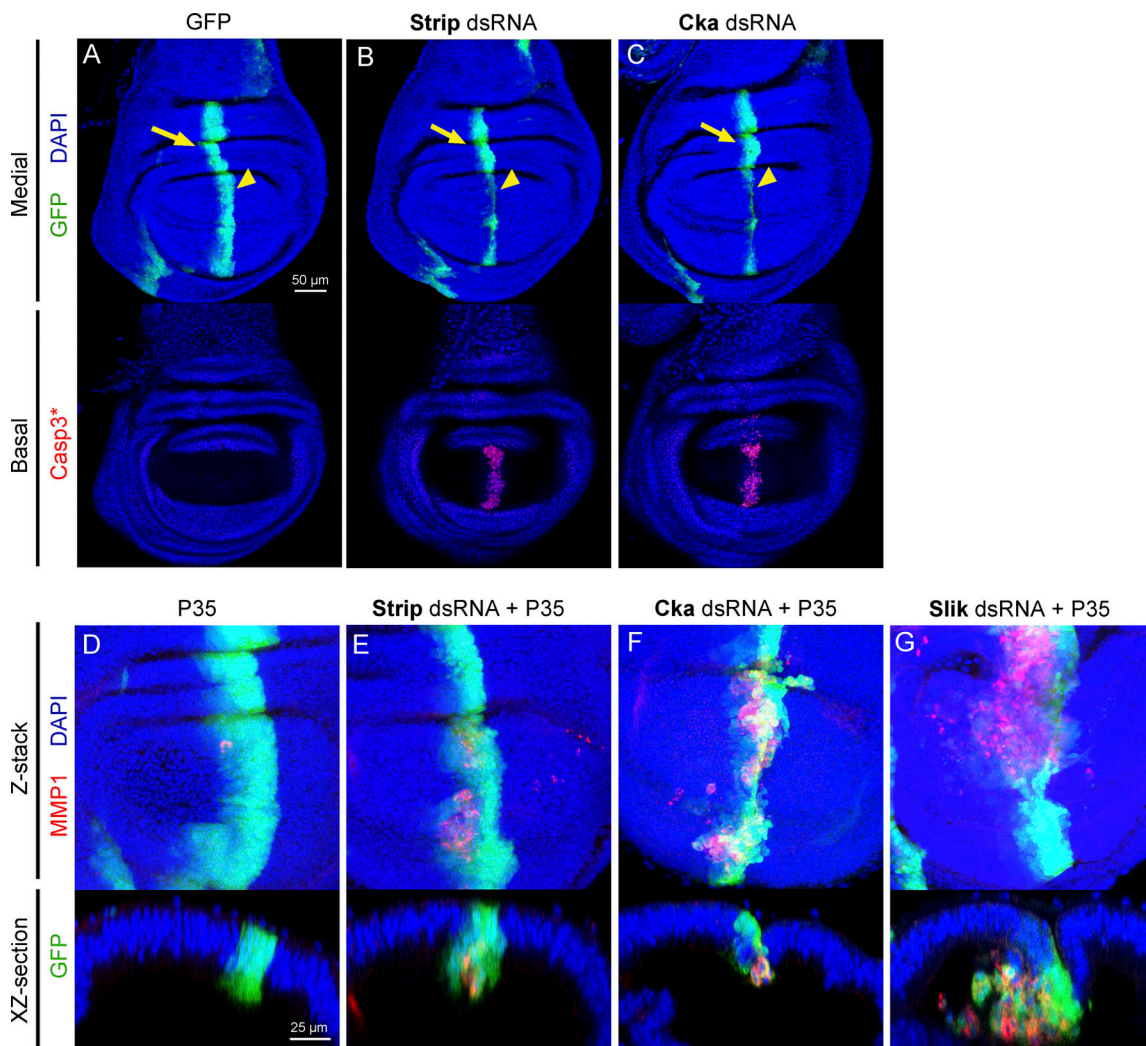
Figure 8. **Strip and Cka control epithelial tissue integrity in *Drosophila* epithelia. (A–C)** Confocal projections through medial (top) or basal (bottom) regions of wing discs expressing GFP (green) in a stripe of cells under control of the *ptc*-GAL4 driver, either alone (A) or together with dsRNA targeting Strip (B) or Cka (C). Discs were stained with DAPI (blue) to visualize nuclei and with anti–cleaved caspase 3 (Casp3) antibody (red) to visualize apoptotic cells. Arrowheads indicate the transgene expression domain within the wing pouch. Arrows indicate the transgene expression domain within the hinge region. **(D–G)** Confocal projections of wing discs (top row) expressing GFP (green) and P35, either alone (D) or together with dsRNA targeting Strip (E), Cka (F), or Slik (G). Discs were stained with DAPI (blue) to visualize nuclei and with anti-MMP1 antibody (red). x–z sections of the same discs (bottom row) generated by orthogonal projection.

similar reduction of p-moesin in Cka-depleted cells in the wing pouch region (Fig. S4 A). Total moesin levels in the *ptc* domain of the hinge region were similar to those in adjacent cells (Fig. S4, B–D, quantified in Fig. S4, H–J), indicating that it was specifically phosphorylation that was affected. The levels and distribution of *Drosophila* E-cadherin (Shotgun, or Shg) were also similar in all three backgrounds (Fig. S4, E–G, quantified in Fig. S4, K–M). This suggests that the changes in p-moesin levels were not due to a global alteration of epithelial polarity.

We next examined the effect of Strip or Cka depletion on Slik localization in cells of the wing hinge region. In wild-type discs, Slik localizes uniformly within and outside of the *ptc* domain, with increased protein accumulation evident at both the apical and basal sides of the epithelial cells (Fig. 9 G, quantified in Fig. 9, J and K). In Strip- or Cka-depleted cells, the intensity of

Slik staining was reduced (Fig. 9, H and I). However, this effect was not uniform. Compared with neighboring wild-type cells, Slik levels in the apical half of STRIPAK-depleted cells were unchanged (Fig. 9, L and N). However, the levels in the basal half of depleted cells were significantly lower (Fig. 9, M and O). We conclude that dSTRIPAK controls the subcellular localization of Slik and consequently its ability to phosphorylate moesin in imaginal disc epithelial cells, as in S2 cells.

To confirm that the effects on moesin phosphorylation were due to altered Slik function, we tested the effect of Strip or Cka depletion in Slik-overexpressing cells. Expression of Slik in the *ptc* domain strongly increased moesin phosphorylation (Fig. 10 A). This was largely suppressed by Strip or Cka depletion (Fig. 10, B and C, quantified in Fig. 10 D). Thus, as is S2 cells, the ability of Slik to phosphorylate moesin is dependent on STRIPAK.
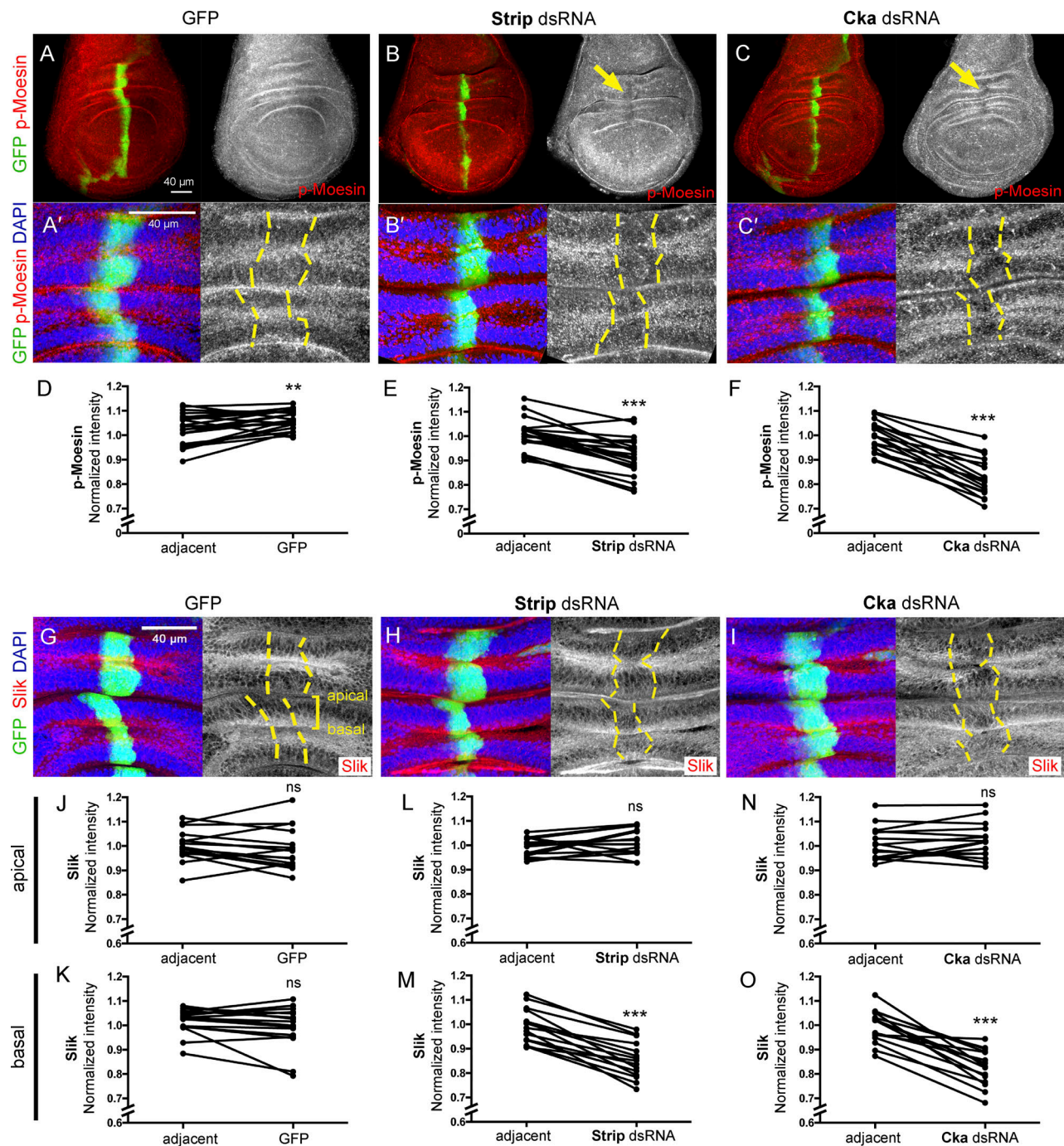
Figure 9. **Strip and Cka control Slik localization and function in the wing disc epithelium. (A–C)** Confocal projections through medial regions of wing discs expressing GFP (green) in a stripe of cells under control of the *ptc*-GAL4 driver, either alone (A) or together with dsRNA targeting Strip (B) or Cka cDNA (blue) and p-moesin (red). Arrows indicate downregulation of p-moesin levels in dSTRIPAK-depleted cells in the wing hinge region. Images in A′–C′ show higher-magnification projections of the hinge region. Yellow dotted lines indicate limits of the GFP-transgene expression domains. **(D–F)** Quantification of normalized p-moesin fluorescence intensity in hinge cells expressing GFP alone (D) or together with dsRNA targeting Strip (E) or Cka (F) compared with their respective adjacent wild-type (GFP–) cells. Fluorescence was measured at multiple folds in five wing discs for each genotype. Two-tailed paired sample *t* test. **(G–I)** Confocal projections through the hinge region of wing discs expressing GFP (green) alone (G) or together with dsRNA targeting Strip (H) or Cka (I). Discs were stained with DAPI (blue) to visualize nuclei and antibody against Slik (red). Yellow dotted lines indicate limits of the GFP-transgene expression domains. **(J–O)** Quantification of normalized Slik fluorescence intensity in hinge cells as above. Measurements were taken in the apical (J, L, and N) or basal (K, M, and O) halves of the cells at multiple folds in four wing discs for each genotype. Two-tailed paired *t*-test. P values are as follows: NS, P > 0.05; **, P < 0.01; ***, P < 0.001.
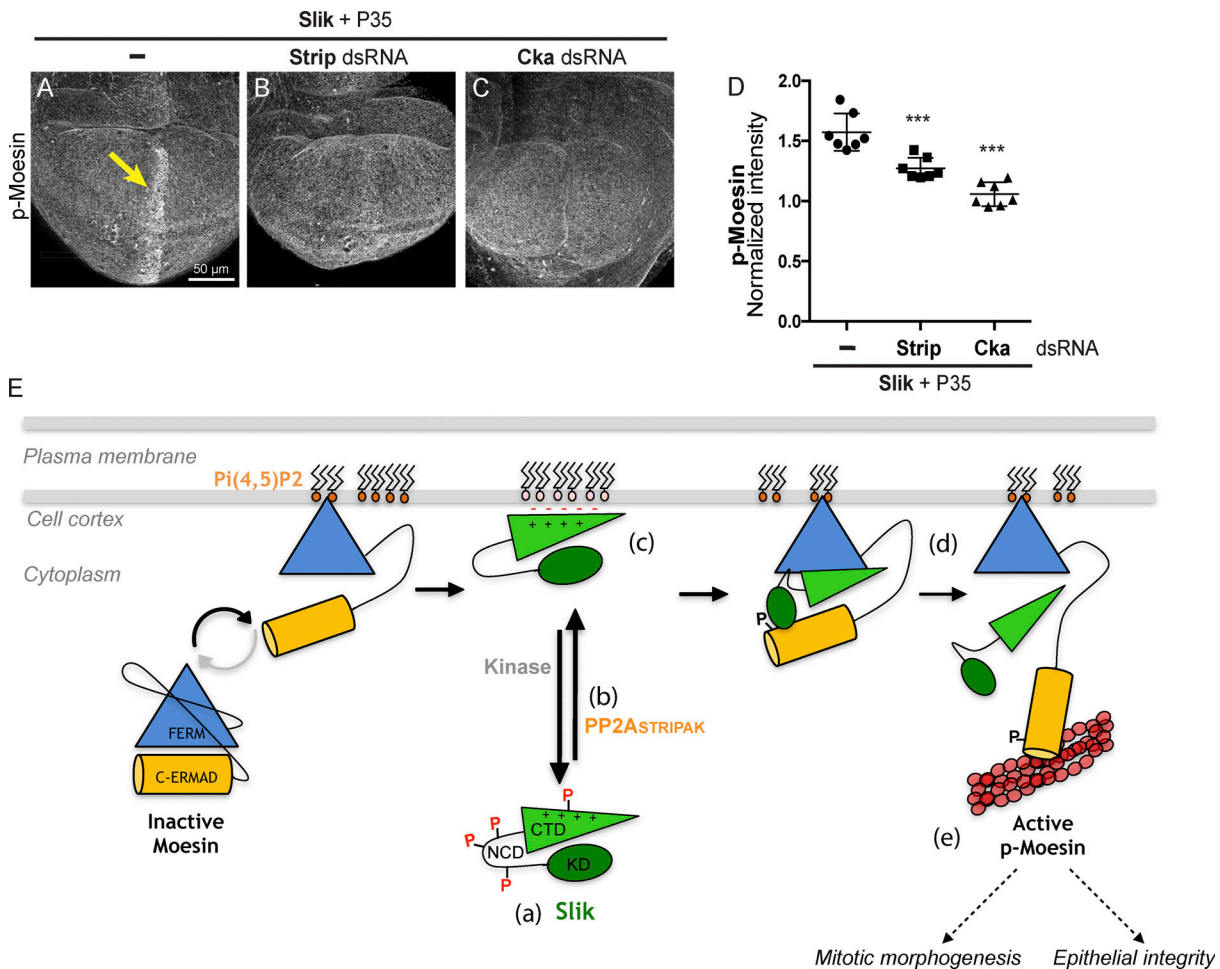
Figure 10. **The ability of Slik to phosphorylate moesin in discs depends on PP2A$_{STRIPAK}$.** **(A–C)** Wing discs overexpressing Slik alone (A) or together with dsRNA targeting Strip (B) or Cka (C) in a stripe of cells under control of the *ptc*-GAL4 driver. Discs were stained with antibody against p-moesin. Images are maximum projections of 56–66 confocal sections spanning the entire thickness of the disc. Arrow indicates upregulation of p-moesin levels in Slik-overexpressing cells. **(D)** Quantification of p-moesin fluorescence intensity in cells in the *ptc* stripe normalized to wild-type posterior compartment cells in discs of the genotypes in A–C. Measurements were made in 7 wing discs for each genotype. Two-tailed unpaired *t* test with P value: ***, P < 0.0001. **(E)** Model for the regulation of Slik localization at the cell cortex (adapted from Pelaseyed et al., 2017). Cycle of phosphorylation/dephosphorylation of Slik serves as an electrostatic switch that controls Slik cortical association. (a) Phosphorylated Slik is localized in the cytoplasm due to electrostatic repulsion with the negatively charged plasma membrane. (b) dSTRIPAK phosphatase activity (PP2A$_{STRIPAK}$) dephosphorylates Slik and promotes its association with the cortex. (c) The polybasic CTD is responsible for Slik localization at the cortex through electrostatic interaction. (d) Once at the cell cortex, Slik can phosphorylate the PtdIns(4,5)P$_2$-primed moesin on its T559. (e) Activated moesin is essential for proper mitotic morphogenesis and epithelial integrity.

Discussion

We discovered that dSTRIPAK dephosphorylates Slik to favor its association with the cortex. This regulation of Slik cortical association occurs both in interphase and in metaphase. Importantly, loss of Slik cortical association correlates with a decreased activation of moesin, the substrate of Slik throughout the cell cycle. Finally, we showed that dSTRIPAK controls moesin-related biological functions such as mitotic morphogenesis and epithelial integrity during development.

dSTRIPAK is a multimolecular complex that functionally bridges PP2A phosphatase activity with kinases of the Ste20-like family (Kück et al., 2019). PP2A$_{STRIPAK}$ was shown to inhibit the catalytic activity of its associated kinases (Gordon et al., 2011; Hyodo et al., 2012; Ribeiro et al., 2010; Zheng et al., 2017). For instance, PP2A$_{STRIPAK}$ dephosphorylates key regulatory residues of the activation loop of Hippo and Mst3/4 (Gordon et al., 2011;

Ribeiro et al., 2010). Here, we found a new functional interaction between PP2A$_{STRIPAK}$ and an Ste20-like kinase. PP2A$_{STRIPAK}$ regulates Slik phosphorylation to control its association with the cortex and thereby regulates its activity toward moesin. PP2A$_{STRIPAK}$ could indirectly regulate an upstream regulator of Slik or directly dephosphorylate this Ste20-like kinase. We favor the latter hypothesis because we found that Slik associates with Cka and Strip, two major components of PP2A$_{STRIPAK}$.

It is unlikely that PP2A$_{STRIPAK}$ dephosphorylates the regulatory residues of the activation loop of Slik, because we did not measure any change of its kinase activity upon depletion of key components of PP2A$_{STRIPAK}$. We then focused on 21 other potential phosphosites, and we discovered that PP2A$_{STRIPAK}$ favors association of Slik with the cortex by regulating some of these phosphosites. Replacing these potentially phosphorylated residues by nonphosphorylatable alanine either within the NCD or

within the CTD of Slik is sufficient to promote the cortical enrichment of these two phosphodeficient mutants and to prevent their regulation by PP2A$_{STRIPAK}$. Importantly, both these mutants rescue or partially rescue the decrease in moesin phosphorylation observed after PP2A$_{STRIPAK}$ depletion. Although these experiments demonstrate that global phosphorylation governs the association of Slik with the cortex, the sites regulated by PP2A$_{STRIPAK}$ remain to be precisely identified.

We previously found that the CTD of Slik is necessary and sufficient for its association with the cell cortex (Panneton et al., 2015). Interestingly, this domain is polybasic (with a theoretical isoelectric point of ~9.6 compared with Slik ~6.1). As previously demonstrated for other signaling proteins (Das et al., 2003; Thelen et al., 1991), these positive charges could promote the association of Slik with the negatively charged inner leaflet of the plasma membrane (Goldenberg and Steinberg, 2010; Kurotani et al., 2019). We propose that the global negative charge brought by phosphorylation promotes the dissociation of Slik with the cell cortex by electrostatic repulsion with the negatively charged plasma membrane. In this model, a cycle of phosphorylation–dephosphorylation of Slik serves as an electrostatic switch that controls Slik cortical association. We previously reported that Slik can be phosphorylated by other not yet identified kinases (Panneton et al., 2015). Consistent with this, we found that OA treatment promotes phosphorylation of a Slik kinase dead mutant even in the absence of endogenous Slik (unpublished results). We therefore favor the hypothesis that one or more other kinases regulate the association of Slik with the cortex. Our current efforts aim to identify which kinase(s) could promote the dissociation of Slik from the plasma membrane (Fig. 10 E).

PP2A phosphatase activity plays important roles during mitosis. Independently of STRIPAK, PP2A regulates mitotic exit by dephosphorylating Cdk1 substrates when associated with the B55 regulatory subunit (*Drosophila* Tws). When associated with the B56 regulatory subunit (*Drosophila* Wdb), PP2A controls spindle organization by counteracting several kinases, such as Aurora-B or Plk1 (Nilsson, 2019). However, only a few studies reported a role of PP2A$_{STRIPAK}$ during mitosis. In mammalian cells, PP2A$_{STRIPAK}$ regulates abscission by controlling Mink1 activity (Hyodo et al., 2012), and depletion of STRIP or striatin promotes cytokinesis failures (Frost et al., 2012). Here, we discovered that PP2A$_{STRIPAK}$ controls mitotic morphogenesis. Mitotic cell morphogenesis requires that moesin be activated at mitosis onset (Ramkumar and Baum, 2016). We found that PP2A$_{STRIPAK}$ controls enrichment of Slik at the cortex of metaphase cells and subsequent moesin activation.

Moesin and Slik play an important role in promoting epithelial integrity in vivo, although the details of their regulation in this context are also poorly understood. In mitotic epithelial cells, p-moesin accumulates at the basolateral membrane and is needed for planar spindle orientation. Moesin-depleted cells frequently undergo mitoses perpendicular to the plane of the epithelium, with the daughter cells undergoing EMT and delaminating and ultimately being eliminated by apoptosis (Nakajima et al., 2013). This appears to be a major cause of the loss of epithelial tissue integrity in *moesin* mutants (Nakajima

et al., 2013; Speck et al., 2003). Several of our observations implicate dSTRIPAK in promoting moesin activation and epithelial tissue integrity. We found that dSTRIPAK-depleted cells undergo EMT, delaminate, and are eliminated by apoptosis, particularly those located in the wing pouch. In dSTRIPAK-depleted cells in the wing hinge region that maintained their epithelial phenotype, we observed reduced levels of p-moesin, a readout for Slik activity. This was not just correlative; the ability of overexpressed Slik to phosphorylate moesin depended on dSTRIPAK. Finally, dSTRIPAK-depleted cells showed a redistribution of Slik protein, with a reduction of protein levels particularly prominent in the basal half of the cells. Together, these results support the finding that dSTRIPAK is a general regulator of Slik localization to promote the morphogenetic functions of moesin. We note that the phenotypic consequences of interfering with dSTRIPAK were more severe than those observed upon depletion of Slik, with strong dSTRIPAK depletion causing early lethality. This suggests that dSTRIPAK regulates other targets, consistent with its known role in down-regulating the growth-inhibitory function of Hippo (Ribeiro et al., 2010; Zheng et al., 2017). Hippo signaling is particularly important for growth of the wing blade (Zecca and Struhl, 2010), which may explain why depletion of dSTRIPAK components had a stronger effect in the wing pouch than in hinge regions.

In conclusion, we identified that PP2A$_{STRIPAK}$ regulates the localization of Slik by phosphorylation to control moesin activation. Our work places STRIPAK as a critical upstream regulator of moesin function for mitotic morphogenesis and epithelial integrity.

Materials and methods

Primary and secondary screens

Primary and secondary screens were performed in 96-well plates (BD Biosciences). 20×10^3 S2 cells per well were plated in 200 µl Schneider medium and treated with 2 µg of dsRNA (Open Biosystems *Drosophila* Library 2.0). After 5 d of incubation at 27°C, cells were fixed in 10% TCA and incubated overnight with an antibody against p-ERM (1:1,000; Cell Signaling Technology). Cells were then incubated with a goat Alexa Fluor 488–conjugated secondary antirabbit antibody (1:400, A11070; Invitrogen). Texas Red-X Phalloidin (1:600, T7471; Invitrogen) and DAPI were used to stain cytoplasm and nuclei, respectively. Cells were mounted with MOWIOL mounting medium (BioShop Canada). Images were acquired at 20× magnification using an Operetta high-content analysis system (PerkinElmer) and analyzed using Harmony high-content analysis software (PerkinElmer). Cells were detected by analyzing the nucleus (DAPI) and cytoplasm (phalloidin). Mean intensity of p-moesin levels per cell ($\overline{x_i}$) was then measured. A score ($Score_i$) was calculated for each condition (i) as follows:

$$Score_i = \frac{X_i}{Median_{Platej}(X_i)},$$

where X_i corresponds to the percentage of cells whose mean intensity of p-moesin level is superior to a threshold (k). k was determined by studying the distribution of cell populations upon

De Jamblinne et al.
STRIPAK regulates moesin functions

Journal of Cell Biology 15 of 19
https://doi.org/10.1083/jcb.201911035

treatment with negative (GFP) and positive (moesin) control dsRNAs in order to match the following condition:

$$\% of cells in Well_{CTRLneg} with \overline{x}_i > k \approx 80\%.$$

dsRNA production and primers

dsRNAs were produced by reverse transcription using the RiboMAX Express Large Scale RNA Production System (P1320; Promega). dsRNAs targeting moesin, PP1-87B, Slik, and Slik 5′UTR were previously reported (Carreno et al., 2008; Panneton et al., 2015; Roubinet et al., 2011). dsRNAs against Tws, Wdb, Wrd, and PP2A-B″ were kindly provided by V. Archambault (IRIC, Montreal, Canada; Chen et al., 2007). Other dsRNAs were amplified from genomic DNA or cDNA (see Data S1, experimental procedures section, for dsRNA primer sequences).

Confirmation miniscreens

dsRNA-treated cells were incubated with an antibody against p-ERM (1:1,000; Cell Signaling Technology) and an antibody against p-histone H3 (1:1,000, clone 6G3; Cell Signaling Technology). Cells were then incubated with a goat Alexa Fluor 488–conjugated anti-rabbit secondary antibody (1:400, A11070; Invitrogen) and a Texas Red–conjugated goat anti-mouse secondary antibody (1:200, T862; Invitrogen). Cells were detected by analyzing the nucleus (DAPI), and interphase cells (p-histone H3 negative) were distinguished from mitotic cells (p-histone H3 positive). The mean intensity of p-moesin levels per cell was then measured in each cell population as described for the screens.

cDNA constructs

Moesin-GFP and Slik[WT]-GFP were previously described (Carreno et al., 2008; Roubinet et al., 2011). Stag-Cka and Stag-Strip were kindly provided by M. Therrien (IRIC, Montreal, Canada; Ashton-Beaucage et al., 2014). Slik[NCD*] and Slik[CTD*] were obtained using cDNA synthesized by Genescript (see Data S2, experimental procedures section, for cDNA sequences). The two mutated sequences were then cloned into pMet-Slik-GFP and replaced the wild-type sequences.

S2 cell culture, dsRNA treatment, transfection, or drug treatments

Drosophila S2 cells were grown at 27°C in Gibco Schneider's *Drosophila* medium (21720001; Life Technologies) complemented with 10% FBS (12483020; Invitrogen) and 5% Gibco penicillin-streptomycin antibiotics (15070063; Life Technologies). For knockdown experiments, 1.5×10^6 cells were treated with 15 μg of dsRNA during 5 d. For overexpression, cells were transfected with the indicated cDNA using FuGENE HD reagent (E2311; Promega) and analyzed 36 to 72 h after transfection. For immunofluorescence or Western blot analysis, cells were treated for 60 min with 10 nM OA (OKA004; BioShop Canada) or 30 min with 100 nM OA or for 60 min with 50 nM Stau (A8192; APExBIO). For live-cell analysis, stable cell lines were treated with 50 nM OA or 50 nM Stau.

S2 stable cell lines and time-lapse microscopy

The stable cell line expressing moesin-GFP in combination with α-tubulin-mCherry has been described previously (Roubinet et al., 2011). Stable cell lines expressing Slik[WT/NCD*/CTD*]-GFP (under pMt promoter) were generated upon Gibco Hygromycin B (Thermo Fisher Scientific) selection. Slik[WT/NCD*/CTD*]-GFP expression was induced with copper sulfate ($CuSO_4$; 0.7mM), and cells were analyzed 36 h after induction. For time-lapse microscopy, 50×10^3 cells were plated in 96-well glass-bottom plates (82050-792, SensoPlate microplate; Greiner Bio-One) and filmed either overnight (dsRNA treatments) or for 1 h (drug treatments) in an environmental chamber at 27°C in Schneider's medium. Cells expressing moesin-GFP were imaged using a DeltaVision inverted microscope (Olympus) with a Plan Apochromat 60×/1.42 NA oil lens (equipped with a CoolSNAP HQ2 camera) and controlled by SoftWoRx software. Cells expressing Slik-GFP were imaged using a Carl Zeiss confocal spinning disk microscope with a Plan Apochromat 63×/1.4 NA oil differential interference contrast lens (equipped with a Zeiss Axiocam 506 mono camera) and controlled using ZEN 2 blue software (Carl Zeiss Microscopy). Representative images were prepared for publication using SoftWoRx, ImageJ (National Institutes of Health), and Photoshop (Adobe) software.

Immunostaining, imaging, and image analysis of S2 cells

S2 cells were plated on glass coverslips and fixed with 4% paraformaldehyde (Alfa Aesar) for 30 min. Cells were permeabilized and blocked with TBS containing 0.1% Triton X-100 and 1% BSA and incubated overnight with antibody against Slik (1:2,000; Panneton et al., 2015). Cells were then incubated with an Alexa Fluor 488–conjugated goat anti–guinea pig secondary antibody (1:100, A11073; Invitrogen). Texas Red-X Phalloidin (1:100, T7471; Invitrogen) was used to stain F-actin. Coverslips were mounted in VECTASHIELD medium with DAPI (Vector Laboratories). Images were acquired using a Nikon Eclipse Ti inverted microscope with a 63×/0.45 NA oil differential interference contrast lens (equipped with an extra–long-working distance camera) and controlled using MetaMorph 6.1 software (Molecular Devices). Representative images were prepared for publication using ImageJ and Photoshop software. Mean fluorescence intensities of Slik and SlikWT/NCD*/CTD*-GFP were measured at the cortex and in the cytoplasm using ImageJ software. Background was measured and subtracted. The ratios correspond to the mean intensity at the cortex over the mean intensity in the cytoplasm. The normalized data were then plotted using Prism software (GraphPad Software). The values for each single cell are represented as dots; independent experiments are shown as circles.

Cell lysis, SDS-PAGE, and Western blot analysis

2×10^6 cells were centrifuged, and pellets were suspended in Laemmli buffer supplemented with antiphosphatases (Phosphatase Inhibitor Cocktail, MilliporeSigma; 1 mM Na_3VO_4; and 5 mM β-glycerophosphate) and antiproteases (1 mM PMSF). Antibodies against T559–p-moesin (1:1,000), moesin (1:25,000; Roubinet et al., 2012), Strip (1:400, kindly provided by T. Chihara, University of Tokyo, Tokyo, Japan; Sakuma et al., 2016), Cka (1:200, kindly provided by T.S. Hays, University of Minnesota, Minneapolis, MN; Neisch et al., 2017), β-actin (1:5,000, clone 4; MilliporeSigma), or α-tubulin (1:1,000, clone DM1A;

MilliporeSigma). For Western blot quantification, the immunoreactive bands were quantified by densitometric analysis using ImageJ software. Backgrounds were subtracted. Normalization was performed as described in the figure legends.

For λ-phosphatase assays, cell pellets were suspended in Triton lysis buffer (1 mM EDTA, 150 mM NaCl, 50 mM Tris-HCl, pH 7.2, 10% glycerol, 0.2% Triton X-100, 1 mM PMSF, aprotinine, and leupeptine) complemented with either phosphatase inhibitors (Phosphatase Inhibitor Cocktail, MilliporeSigma; and 1 mM Na$_3$VO$_4$) or λ-phosphatase (P0753S; New England Biolabs). The reaction was incubated at 30°C for 60 min and stopped in Laemmli buffer at 95°C. For Slik mobility shift assay, cell lysates were resolved using a precast 3–8% gradient SDS-PAGE gel (EA0375BOX; Invitrogen). The membranes were blocked with TBS–0.1% Tween containing 5% milk (Carnation; Nestlé) and then incubated with rabbit antibody against Slik (1:1,000). Line scans were performed by densitometric analysis of Slik immunoreactive bands using ImageJ software. The proportion of shifted Slik bands was evaluated by the ratio of the area under the line scan curves (upward shifted/unshifted) of Slik in different conditions. Data of independent experiments (shown as circles) were plotted using Prism software.

Coimmunoprecipitation assays
8×10^6 cells were lysed 72 h post-transfection in 400 µl of Triton lysis buffer (1 mM EDTA, 150 mM NaCl, 50 mM Tris-HCl, pH 7.2, 10% glycerol, and 0.2% Triton X-100) supplemented with anti-phosphatases (Phosphatase Inhibitor Cocktail, MilliporeSigma; 1 mM Na$_3$VO$_4$, 5 mM β-glycerophosphate, 1 mM PMSF) and antiprotease cocktail (DA36046; Roche). GFP-Trap beads (Chromotek) or anti-Stag (A00625; Genescript) along with protein A agarose beads (17-0780-01; GE Healthcare Life Sciences) were added to cell lysates and gently rocked at 4°C for 2 h or 4 h, respectively. The immunoprecipitates were resolved on SDS-PAGE gels and immunoblotted with antibodies against GFP (1:2,500; Invitrogen), Stag (1:1,000; Genescript), or Flag (Western blot 1:4,000, clone M2; MilliporeSigma).

In vitro kinase assay
5×10^6 cells were lysed in 400 µl of Tris lysis buffer (40 mM Hepes, 1 mM EDTA, 120 mM NaCl, 10 mM tetrasodium pyrophosphate, 10% glycerol, 1% Triton X-100, and 0.1% SDS) supplemented with antiphosphatases (Phosphatase Inhibitor Cocktail, MilliporeSigma; 1 mM Na$_3$VO$_4$, 5 mM β-glycerophosphate, 1 mM PMSF) and antiprotease cocktail (DA36046; Roche). Cell lysates were immunoprecipitated with antibody against Slik for 4 h and then incubated with protein A sepharose beads for 2 h. The beads from immunoprecipitations were subjected to an in vitro kinase assay as previously described (Plutoni et al., 2019).

RNA extraction for quantitative real-time PCR
Total RNA was extracted from *Drosophila* S2 cells using the DNAaway RNA Miniprep Kit (BS88133; Bio Basic). Total RNA was reverse transcribed with a cDNA reverse transcription kit (Applied Biosystems). PCRs were performed on an ABI Real Time 7900HT cycler and analyzed with SDS 2.2 software using

the following probes for our genes of interest and two endogenous control genes (*Act5c* and *Rpl32*) with high efficiency (>95%): Strip forward, 5′-aggccaattacgcggtct-3′, and reverse, 5′-cgcgca tgtggatattagag-3′; Cka forward, 5′-aaggatatgctcaccgagga-3′, and reverse, 5′-gccatcagattcgttattcacc-3′; Act5c forward, 5′-accgag cgcggttactct-3′, and reverse, 5′-cttgatgtcacggacgatttc-3′; Rpl32 forward, 5′-cggatcgatatgctaagctgt-3′, and reverse, 5′-gcgcttgtt cgatccgta-3′. Quantitative real-time PCR was performed with TaqMan Gene Expression Master Mix (Applied Biosystems). mRNA levels of target genes were normalized to the averaged levels of both control genes.

Drosophila stocks and culture
ptc-GAL4 (*ptc*[559.1]), *UAS-GFP*, and *UAS-P35* strains were obtained from the Bloomington *Drosophila* Stock Center. *EP-Slik* (*slik*[20348]) is an EPg element insertion upstream of the *slik* gene that drives its GAL4-dependent expression. Transgenic dsRNA strains targeting *cka* (ID no. 106971), *strip* (ID no. 106184), and *slik* (ID no. 43783) were obtained from the Vienna *Drosophila* Resource Center. Crosses were performed at 18°C, 21°C, 25°C, or 27°C, as indicated. The genotypes were as follows: *w;ptcGAL4,UAS-GFP/+* at 25°C (Figs. 8 A, 9 A, and 9 G); *w;ptcGAL4,UAS-GFP/UAS-strip.dsRNA* at 25°C (Figs. 8 B, 9 B, and 9 H); *w;ptcGAL4,UAS-GFP/ UAS-cka.dsRNA* at 25°C (Figs. 8 C, 9 C, and 9 I); *w,UAS-P35; ptcGAL4,UAS-GFP/+* at 25°C (Fig. 8 D); *w,UAS-P35;ptcGAL4,UAS-GFP/UAS-strip.dsRNA* at 25°C (Fig. 8 E); *w,UAS-P35;ptcGAL4, UAS-GFP/UAS-cka.dsRNA* at 18°C (Fig. 8 F); *w,UAS-P35;ptcGAL4, UAS-GFP/UAS-slik.dsRNA* at 27°C (Fig. 8 G); *w,UAS-P35;ptcGA-L4,EP-Slik/+* at 21°C (Fig. 10 A); *w,UAS-P35;ptcGAL4,EP-Slik/UAS-strip.dsRNA* at 21°C (Fig. 10 B); and *w,UAS-P35;ptcGAL4,EP-Slik/ UAS-cka.dsRNA* at 18°C (Fig. 10 C).

Immunostaining, imaging, and image analysis of imaginal discs
Wandering third instar larvae were dissected, and anterior halves with attached wing discs were collected in PBS on ice. Discs were fixed in PBS containing 0.2% Tween-20 (PBT) and 4% formaldehyde for 20 min. After several washes with PBT, samples were blocked in PBT with 0.1% BSA, followed by incubation overnight at 4°C with primary antibodies against Slik (1:1,000), p-moesin (1:100), GFP (1:100, TP401; OriGene Technologies), cleaved caspase 3 (1:150, no. 9661; Cell Signaling Technology), MMP1 (1:100; 1:1 mix of Developmental Studies Hybridoma Bank [DSHB] nos. 3A6B4 and 5H7B11), Ptc (1:1,000, Apa-1; DSHB), Shg (1:200, DCAD2; DSHB), and moesin (1:4,000; a gift from Daniel Kiehart, Duke University, Durham, NC). Samples were incubated with Fluor-conjugated secondary antibodies (Invitrogen and Jackson ImmunoResearch Laboratories). Discs were mounted on slides in mounting medium (10% PBS, 90% glycerol, 0.2% *n*-propyl gallate), coverslipped, and imaged at RT using a Zeiss LSM700 confocal microscope with a Plan Apochromat 20×/0.75 NA lens (Fig. 8, A–C; and Fig. 9, A–C) or a Plan Neofluar 40×/1.30 NA oil lens and controlled using ZEN 2 software. Representative images were prepared for publication using ImageJ and Photoshop software.

We quantified Slik or p-moesin levels using ImageJ software. Mean fluorescence intensities were measured within the GFP-positive cells and a comparable area of adjacent GFP-negative

cells within single layers of the epithelium. The measurement at a nearby third GFP-negative region was used as a normalization control. For Slik measurements, fluorescence intensity was measured separately in the apical and basal halves of the epithelium, using the midpoint of the nuclear layer as the dividing line. The normalized data were plotted using Prism (GraphPad Software).

Statistical analysis

Results are expressed as average ± SD or ± SEM as indicated in the figure legends. Statistical significance between various conditions was assessed by determining P values (with 95% confidence interval) using Prism software. Different tests were performed as indicated in the figure legends: (un)paired Student's *t* test (two experimental groups) and unpaired one-way ANOVA (multiple comparisons test). Parametric tests were used because the distributions across samples were assumed to be normal, but this was not formally tested.

Online supplemental material

Fig. S1 shows that some dSTRIPAK adapter proteins slightly affect moesin phosphorylation and validated dsRNA efficiency for Mts, PP2A-29B, Strip, and Cka. Fig. S2 shows that different Slik isoforms are overphosphorylated in the absence of PP2A$_{STRIPAK}$ without affecting its kinase activity. Fig. S3 presents the independent experiments of the pooled data in Figs. 4 D, 4 F, and 5 B. Fig. S4 shows that Strip or Cka depletion has little effect on total moesin and E-cadherin (shotgun) levels and distribution in wing discs. Table S1 lists the 51 validated genes from the genome-wide RNAi screen and their activation scores. Data S1 shows lists primer sequences. Data S2 shows shows cDNA sequences synthetized for Slik mutants.

References

Ashton-Beaucage, D., C.M. Udell, P. Gendron, M. Sahmi, M. Lefrançois, C. Baril, A.S. Guenier, J. Duchaine, D. Lamarre, S. Lemieux, et al. 2014. A functional screen reveals an extensive layer of transcriptional and splicing control underlying RAS/MAPK signaling in *Drosophila*. *PLoS Biol*. 12. e1001809. https://doi.org/10.1371/journal.pbio.1001809

Bodenmiller, B., and R. Aebersold. 2011. Phosphoproteome resource for systems biology research. *Methods Mol. Biol*. 694:307–322. https://doi.org/10.1007/978-1-60761-977-2_19

Carreno, S., I. Kouranti, E.S. Glusman, M.T. Fuller, A. Echard, and F. Payre. 2008. Moesin and its activating kinase Slik are required for cortical stability and microtubule organization in mitotic cells. *J. Cell Biol*. 180: 739–746. https://doi.org/10.1083/jcb.200709161

Chen, F., V. Archambault, A. Kar, P. Liò, P.P. D'Avino, R. Sinka, K. Lilley, E.D. Laue, L. Capalbo, et al. 2007. Multiple protein phosphatases are required for mitosis in *Drosophila*. *Curr. Biol*. 17:293–303. https://doi.org/10.1016/j.cub.2007.01.068

Cohen, P., S. Klumpp, and D.L. Schelling. 1989. An improved procedure for identifying and quantitating protein phosphatases in mammalian tissues. *FEBS Lett*. 250:596–600. https://doi.org/10.1016/0014-5793(89)80803-8

Das, S., J.E. Dixon, and W. Cho. 2003. Membrane-binding and activation mechanism of PTEN. *Proc. Natl. Acad. Sci. USA*. 100:7491–7496. https://doi.org/10.1073/pnas.0932835100

Elramli, N., B. Karahoda, Ö. Sarikaya-Bayram, D. Frawley, M. Ulas, C.E. Oakley, B.R. Oakley, S. Seiler, and Ö. Bayram. 2019. Assembly of a heptameric STRIPAK complex is required for coordination of light-dependent multicellular fungal development with secondary metabolism in *Aspergillus nidulans*. *PLoS Genet*. 15. e1008053. https://doi.org/10.1371/journal.pgen.1008053

Favre, B., P. Turowski, and B.A. Hemmings. 1997. Differential inhibition and posttranslational modification of protein phosphatase 1 and 2A in MCF7 cells treated with calyculin-A, okadaic acid, and tautomycin. *J. Biol. Chem*. 272:13856–13863. https://doi.org/10.1074/jbc.272.21.13856

Fehon, R.G., A.I. McClatchey, and A. Bretscher. 2010. Organizing the cell cortex: the role of ERM proteins. *Nat. Rev. Mol. Cell Biol*. 11:276–287. https://doi.org/10.1038/nrm2866

Frost, A., M.G. Elgort, O. Brandman, C. Ives, S.R. Collins, L. Miller-Vedam, J. Weibezahn, M.Y. Hein, I. Poser, M. Mann, et al. 2012. Functional repurposing revealed by comparing *S. pombe* and *S. cerevisiae* genetic interactions. *Cell*. 149:1339–1352. https://doi.org/10.1016/j.cell.2012.04.028

Gnad, F., J. Gunawardena, and M. Mann. 2011. PHOSIDA 2011: the post-translational modification database. *Nucleic Acids Res*. 39:D253–D260. https://doi.org/10.1093/nar/gkq1159

Goldenberg, N.M., and B.E. Steinberg. 2010. Surface charge: a key determinant of protein localization and function. *Cancer Res*. 70:1277–1280. https://doi.org/10.1158/0008-5472.CAN-09-2905

Gordon, J., J. Hwang, K.J. Carrier, C.A. Jones, Q.L. Kern, C.S. Moreno, R.H. Karas, and D.C. Pallas. 2011. Protein phosphatase 2A (PP2A) binds within the oligomerization domain of striatin and regulates the phosphorylation and activation of the mammalian Ste20-Like kinase Mst3. *BMC Biochem*. 12:54. https://doi.org/10.1186/1471-2091-12-54

Goudreault, M., L.M. D'Ambrosio, M.J. Kean, M.J. Mullin, B.G. Larsen, A. Sanchez, S. Chaudhry, G.I. Chen, F. Sicheri, A.I. Nesvizhskii, et al. 2009. A PP2A phosphatase high density interaction network identifies a novel striatin-interacting phosphatase and kinase complex linked to the cerebral cavernous malformation 3 (CCM3) protein. *Mol. Cell. Proteomics*. 8:157–171. https://doi.org/10.1074/mcp.M800266-MCP200

Hipfner, D.R., N. Keller, and S.M. Cohen. 2004. Slik Sterile-20 kinase regulates Moesin activity to promote epithelial integrity during tissue growth. *Genes Dev*. 18:2243–2248. https://doi.org/10.1101/gad.303304

Hu, Y., R. Sopko, V. Chung, M. Foos, R.A. Studer, S.D. Landry, D. Liu, L. Rabinow, F. Gnad, P. Beltrao, et al. 2019. iProteinDB: an integrative

database of *Drosophila* post-translational modifications. *G3 (Bethesda)*. 9:1–11. https://doi.org/10.1534/g3.118.200637

Hwang, J., and D.C. Pallas. 2014. STRIPAK complexes: structure, biological function, and involvement in human diseases. *Int. J. Biochem. Cell Biol.* 47:118–148. https://doi.org/10.1016/j.biocel.2013.11.021

Hyodo, T., S. Ito, H. Hasegawa, E. Asano, M. Maeda, T. Urano, M. Takahashi, M. Hamaguchi, and T. Senga. 2012. Misshapen-like kinase 1 (MINK1) is a novel component of striatin-interacting phosphatase and kinase (STRIPAK) and is required for the completion of cytokinesis. *J. Biol. Chem.* 287:25019–25029. https://doi.org/10.1074/jbc.M112.372342

Janssens, V., and J. Goris. 2001. Protein phosphatase 2A: a highly regulated family of serine/threonine phosphatases implicated in cell growth and signalling. *Biochem. J.* 353:417–439. https://doi.org/10.1042/bj3530417

Janssens, V., J. Goris, and C. Van Hoof. 2005. PP2A: the expected tumor suppressor. *Curr. Opin. Genet. Dev.* 15:34–41. https://doi.org/10.1016/j.gde.2004.12.004

Kean, M.J., D.F. Ceccarelli, M. Goudreault, M. Sanches, S. Tate, B. Larsen, L.C. Gibson, W.B. Derry, I.C. Scott, L. Pelletier, et al. 2011. Structure-function analysis of core STRIPAK proteins: a signaling complex implicated in Golgi polarization. *J. Biol. Chem.* 286:25065–25075. https://doi.org/10.1074/jbc.M110.214486

Kim, J.W., C. Berrios, M. Kim, A.E. Schade, G. Adelmant, H. Yeerna, E. Damato, A.B. Iniguez, L. Florens, M.P. Washburn, et al. 2020. STRIPAK directs PP2A activity toward MAP4K4 to promote oncogenic transformation of human cells. *eLife*. 9:e53003. https://doi.org/10.7554/eLife.53003

Koenderink, G.H., and E.K. Paluch. 2018. Architecture shapes contractility in actomyosin networks. *Curr. Opin. Cell Biol.* 50:79–85. https://doi.org/10.1016/j.ceb.2018.01.015

Kück, U., D. Radchenko, and I. Teichert. 2019. STRIPAK, a highly conserved signaling complex, controls multiple eukaryotic cellular and developmental processes and is linked with human diseases. *Biol. Chem.* https://doi.org/10.1515/hsz-2019-0173.

Kunda, P., A.E. Pelling, T. Liu, and B. Baum. 2008. Moesin controls cortical rigidity, cell rounding, and spindle morphogenesis during mitosis. *Curr. Biol.* 18:91–101. https://doi.org/10.1016/j.cub.2007.12.051

Kunda, P., N.T. Rodrigues, E. Moeendarbary, T. Liu, A. Ivetic, G. Charras, and B. Baum. 2012. PP1-mediated Moesin dephosphorylation couples polar relaxation to mitotic exit. *Curr. Biol.* 22:231–236. https://doi.org/10.1016/j.cub.2011.12.016

Kurotani, A., A.A. Tokmakov, K.I. Sato, V.E. Stefanov, Y. Yamada, and T. Sakurai. 2019. Localization-specific distributions of protein pI in human proteome are governed by local pH and membrane charge. *BMC Mol. Cell Biol.* 20:36. https://doi.org/10.1186/s12860-019-0221-4

Kyriakis, J.M. 1999. Signaling by the germinal center kinase family of protein kinases. *J. Biol. Chem.* 274:5259–5262. https://doi.org/10.1074/jbc.274.9.5259

Madsen, C.D., S. Hooper, M. Tozluoglu, A. Bruckbauer, G. Fletcher, J.T. Erler, P.A. Bates, B. Thompson, and E. Sahai. 2015. STRIPAK components determine mode of cancer cell migration and metastasis. *Nat. Cell Biol.* 17:68–80. https://doi.org/10.1038/ncb3083

Mehsen, H., V. Boudreau, D. Garrido, M. Bourouh, M. Larouche, P.S. Maddox, A. Swan, and V. Archambault. 2018. PP2A-B55 promotes nuclear envelope reformation after mitosis in *Drosophila*. *J. Cell Biol.* 217:4106–4123. https://doi.org/10.1083/jcb.201804018

Moreno, C.S., W.S. Lane, and D.C. Pallas. 2001. A mammalian homolog of yeast MOB1 is both a member and a putative substrate of striatin family-protein phosphatase 2A complexes. *J. Biol. Chem.* 276:24253–24260. https://doi.org/10.1074/jbc.M102398200

Nakajima, Y., E.J. Meyer, A. Kroesen, S.A. McKinney, and M.C. Gibson. 2013. Epithelial junctions maintain tissue architecture by directing planar spindle orientation. *Nature*. 500:359–362. https://doi.org/10.1038/nature12335

Neisch, A.L., T.P. Neufeld, and T.S. Hays. 2017. A STRIPAK complex mediates axonal transport of autophagosomes and dense core vesicles through PP2A regulation. *J. Cell Biol.* 216:441–461. https://doi.org/10.1083/jcb.201606082

Nilsson, J. 2019. Protein phosphatases in the regulation of mitosis. *J. Cell Biol.* 218:395–409. https://doi.org/10.1083/jcb.201809138

Panneton, V., A. Nath, F. Sader, N. Delaunay, A. Pelletier, D. Maier, K. Oh, and D.R. Hipfner. 2015. Regulation of catalytic and non-catalytic functions of the *Drosophila* Ste20 kinase Slik by activation segment

phosphorylation. *J. Biol. Chem.* 290:20960–20971. https://doi.org/10.1074/jbc.M115.645952

Pelaseyed, T., R. Viswanatha, C. Sauvanet, J.J. Filter, M.L. Goldberg, and A. Bretscher. 2017. Ezrin activation by LOK phosphorylation involves a PIP₂-dependent wedge mechanism. *eLife*. 6:e22759. https://doi.org/10.7554/eLife.22759

Plutoni, C., S. Keil, C. Zeledon, L.E.A. Delsin, B. Decelle, P.P. Roux, S. Carréno, and G. Emery. 2019. Misshapen coordinates protrusion restriction and actomyosin contractility during collective cell migration. *Nat. Commun.* 10:3940. https://doi.org/10.1038/s41467-019-11963-7

Polesello, C., and F. Payre. 2004. Small is beautiful: what flies tell us about ERM protein function in development. *Trends Cell Biol.* 14:294–302. https://doi.org/10.1016/j.tcb.2004.04.003

Ramkumar, N., and B. Baum. 2016. Coupling changes in cell shape to chromosome segregation. *Nat. Rev. Mol. Cell Biol.* 17:511–521. https://doi.org/10.1038/nrm.2016.75

Ribeiro, P.S., F. Josué, A. Wepf, M.C. Wehr, O. Rinner, G. Kelly, N. Tapon, and M. Gstaiger. 2010. Combined functional genomic and proteomic approaches identify a PP2A complex as a negative regulator of Hippo signaling. *Mol. Cell*. 39:521–534. https://doi.org/10.1016/j.molcel.2010.08.002

Roch, F., C. Polesello, C. Roubinet, M. Martin, C. Roy, P. Valenti, S. Carreno, P. Mangeat, and F. Payre. 2010. Differential roles of PtdIns(4,5)P₂ and phosphorylation in moesin activation during *Drosophila* development. *J. Cell Sci.* 123:2058–2067. https://doi.org/10.1242/jcs.064550

Roubinet, C., B. Decelle, G. Chicanne, J.F. Dorn, B. Payrastre, F. Payre, and S. Carreno. 2011. Molecular networks linked by Moesin drive remodeling of the cell cortex during mitosis. *J. Cell Biol.* 195:99–112. https://doi.org/10.1083/jcb.201106048

Roubinet, C., P.T. Tran, and M. Piel. 2012. Common mechanisms regulating cell cortex properties during cell division and cell migration. *Cytoskeleton (Hoboken)*. 69:957–972. https://doi.org/10.1002/cm.21086

Sakuma, C., M. Okumura, T. Umehara, M. Miura, and T. Chihara. 2016. A STRIPAK component Strip regulates neuronal morphogenesis by affecting microtubule stability. *Sci. Rep.* 5:17769. https://doi.org/10.1038/srep17769

Shi, Z., S. Jiao, and Z. Zhou. 2016. STRIPAK complexes in cell signaling and cancer. *Oncogene*. 35:4549–4557. https://doi.org/10.1038/onc.2016.9

Solinet, S., K. Mahmud, S.F. Stewman, K. Ben El Kadhi, B. Decelle, L. Talje, A. Ma, B.H. Kwok, and S. Carreno. 2013. The actin-binding ERM protein Moesin binds to and stabilizes microtubules at the cell cortex. *J. Cell Biol.* 202:251–260. https://doi.org/10.1083/jcb.201304052

Speck, O., S.C. Hughes, N.K. Noren, R.M. Kulikauskas, and R.G. Fehon. 2003. Moesin functions antagonistically to the Rho pathway to maintain epithelial integrity. *Nature*. 421:83–87. https://doi.org/10.1038/nature01295

Stephens, D.J. 2012. Functional coupling of microtubules to membranes – implications for membrane structure and dynamics. *J. Cell Sci.* 125:2795–2804. https://doi.org/10.1242/jcs.097675

Strack, S., J.T. Cribbs, and L. Gomez. 2004. Critical role for protein phosphatase 2A heterotrimers in mammalian cell survival. *J. Biol. Chem.* 279:47732–47739. https://doi.org/10.1074/jbc.M408015200

Tan, J., K. Oh, J. Burgess, D.R. Hipfner, and J.A. Brill. 2014. PI4KIIIα is required for cortical integrity and cell polarity during *Drosophila* oogenesis. *J. Cell Sci.* 127:954–966. https://doi.org/10.1242/jcs.129031

Tang, Y., M. Chen, L. Zhou, J. Ma, Y. Li, H. Zhang, Z. Shi, Q. Xu, X. Zhang, Z. Gao, et al. 2019. Architecture, substructures, and dynamic assembly of STRIPAK complexes in Hippo signaling. *Cell Discov*. 5:3. https://doi.org/10.1038/s41421-018-0077-3

Thelen, M., A. Rosen, A.C. Nairn, and A. Aderem. 1991. Regulation by phosphorylation of reversible association of a myristoylated protein kinase C substrate with the plasma membrane. *Nature*. 351:320–322. https://doi.org/10.1038/351320a0

Zecca, M., and G. Struhl. 2010. A feed-forward circuit linking Wingless, Fat-Dachsous signaling, and the Warts-Hippo pathway to *Drosophila* wing growth. *PLoS Biol*. 8. e1000386. https://doi.org/10.1371/journal.pbio.1000386

Zheng, Y., B. Liu, L. Wang, H. Lei, K.D. Pulgar Prieto, and D. Pan. 2017. Homeostatic control of Hpo/MST kinase activity through autophosphorylation-dependent recruitment of the STRIPAK PP2A phosphatase complex. *Cell Rep*. 21:3612–3623. https://doi.org/10.1016/j.celrep.2017.11.076
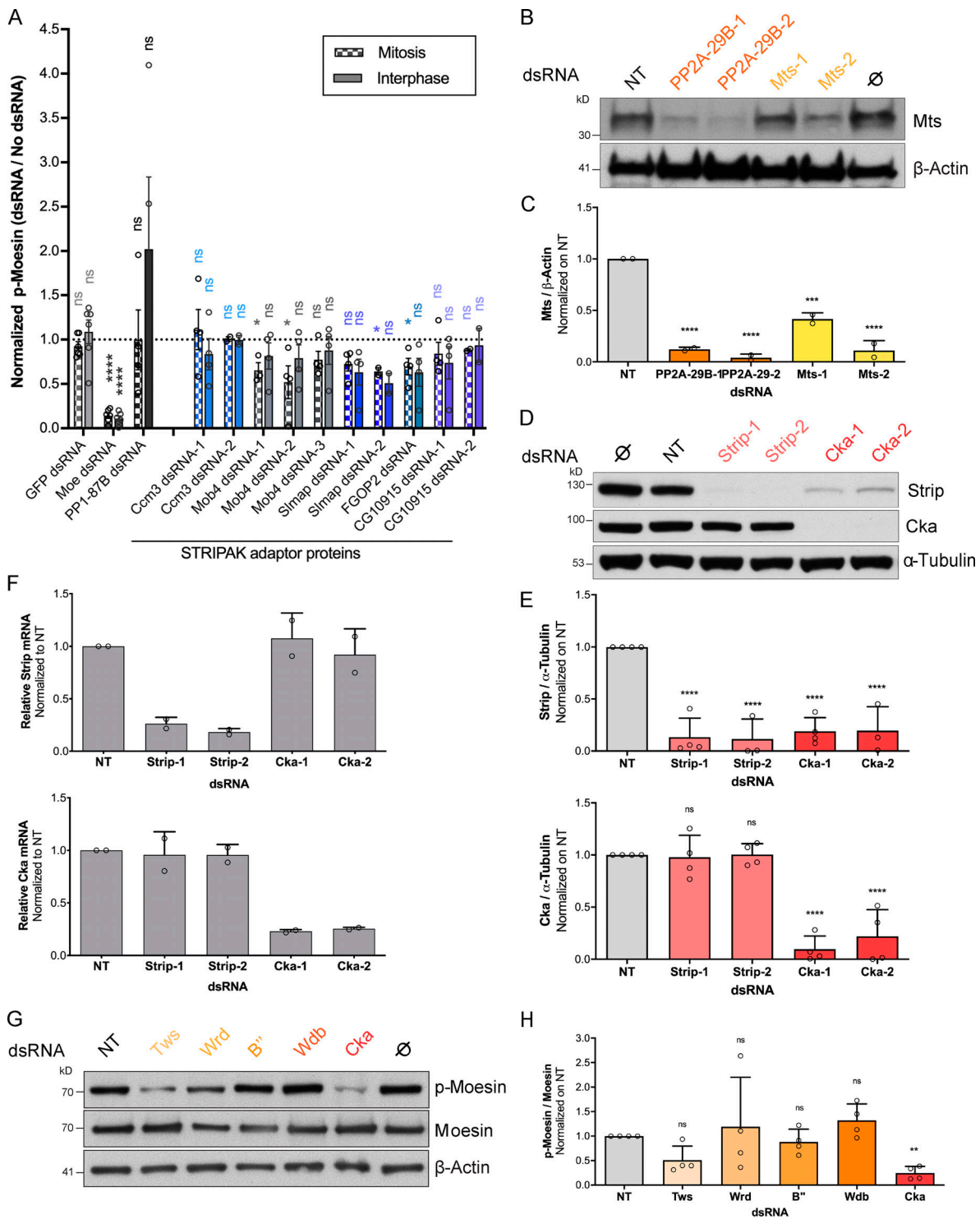
Supplemental material

Figure S1. **Depletion of Mob4, Slmap and FGOP2, three dSTRIPAK adaptor proteins, slightly decrease p-moesin levels. (A)** Automated quantification of the immunofluorescence intensity of p-moesin in S2 cells treated as indicated and normalized to nontreated condition. Data are represented as normalized mean ± SEM of two to four independent experiments (circles). Two-tailed unpaired *t* tests were calculated against the nontreated condition with the following P values: NS, P > 0.05; *, P < 0.05. **(B and D)** Western blot of S2 cells, treated as indicated, with antibodies against Strip, Cka, Mts, and β-actin or α-tubulin. Knockdown of PP2A-29B destabilizes Mts as previously described in mammalian cells ([Strack et al., 2004](#)). Knockdown of Cka destabilizes Strip. **(C and E)** Relative Strip, Cka, or Mts levels (normalized as indicated) were quantified in two to four independent experiments (circles). Data are represented as mean ± SD normalized on nontarget (NT) dsRNA, one-way ANOVA with the following P values: NS, P > 0.05; **, P < 0.01; ****, P < 0.0001. **(F)** Relative Strip or Cka mRNA levels (normalized to *Act5c* and *Rpl32*) were quantified by quantitative real-time PCR in total RNA extracts of S2 cells treated with indicated dsRNA. **(G)** Western blot of S2 cells treated as indicated with antibodies against T559-phosphorylated p-moesin, moesin, and β-actin. **(H)** Relative p-moesin levels (normalized to moesin) were quantified in four independent experiments (circles). Data are represented as mean ± SD normalized on NT dsRNA, one-way ANOVA with the following P values: NS, P > 0.05; **, P < 0.01.
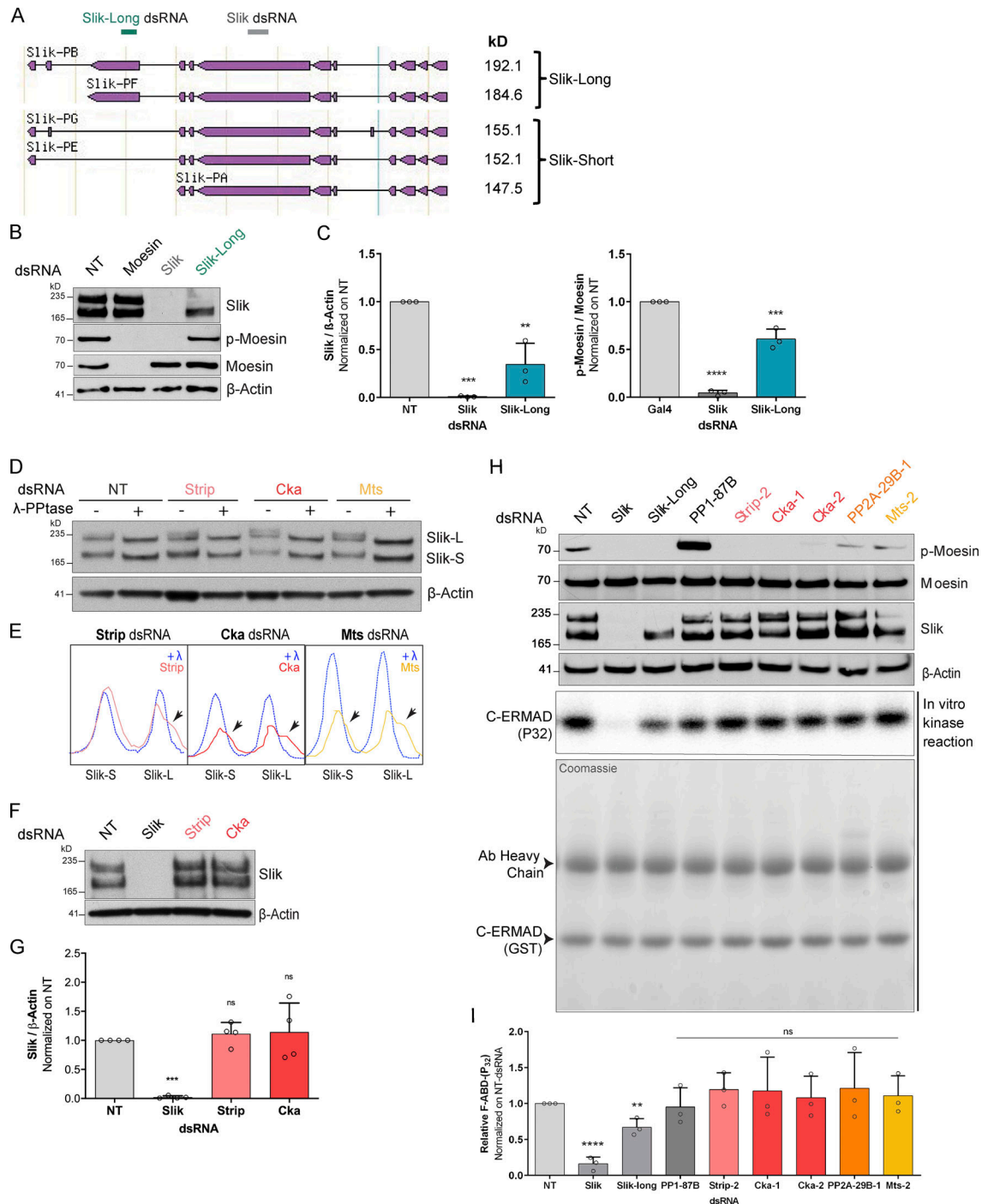
Figure S2. Slik isoforms are overphosphorylated in absence of PP2A$_{STRIPAK}$ without affecting its kinase activity. (A) Schematic representation of Slik mRNA splicing variants (adapted from http://flybase.org/reports/FBgn0035001) and their expected molecular weight (kD). The longer isoforms (Slik-L) code for an additional C-terminal NCD compared with the shorter isoforms (Slik-S). dsRNA designed against all Slik isoforms or specific to Slik-L are indicated. **(B and F)** S2 cells treated as indicated were analyzed by Western blotting with antibodies against Slik, p-moesin, moesin, or β-actin. The upper bands correspond to Slik-L and lower bands to Slik-S isoforms. **(C and G)** Relative Slik or relative p-moesin levels (normalized as indicated) were quantified in three or four independent experiments (circles). Data are represented as mean ± SD normalized on nontarget (NT) dsRNA, one-way ANOVA with the following P values: NS, $P > 0.05$; **, $P < 0.01$; ***, $P < 0.001$; ****, $P < 0.0001$. **(D)** S2 cells treated as indicated were lysed either in the absence (−) or presence (+) of λ-PPtase. Protein extracts were then analyzed by Western blotting using antibodies against Slik or β-actin. **(E)** Representation of the line scans of Western blots on Slik signals (bottom to top). The shifted Slik-L or Slik-S signals are indicated with arrows. **(H)** Western blot of S2 cells, treated as indicated, with antibodies against p-moesin, moesin, Slik, or β-actin (upper rows). Immunoprecipitated Slik from the treated cell lysates was incubated with purified moesin C-ERMAD-GST in a kinase reaction with [γ-^{32}P]ATP. The resulting samples were subjected to SDS–PAGE, and the dried Coomassie-stained gel was autoradiographed (middle and bottom rows). **(I)** Autoradiographed signals of moesin C-ERMAD(P$_{32}$)-GST were quantified in three independent experiments (circles). Data are represented as mean ± SD normalized on nontreated dsRNA, one-way ANOVA with the following P values: NS, $P > 0.05$; **, $P < 0.01$; ****, $P < 0.0001$. NT, non-target; F-ABD, F-Actin Binding Domain.
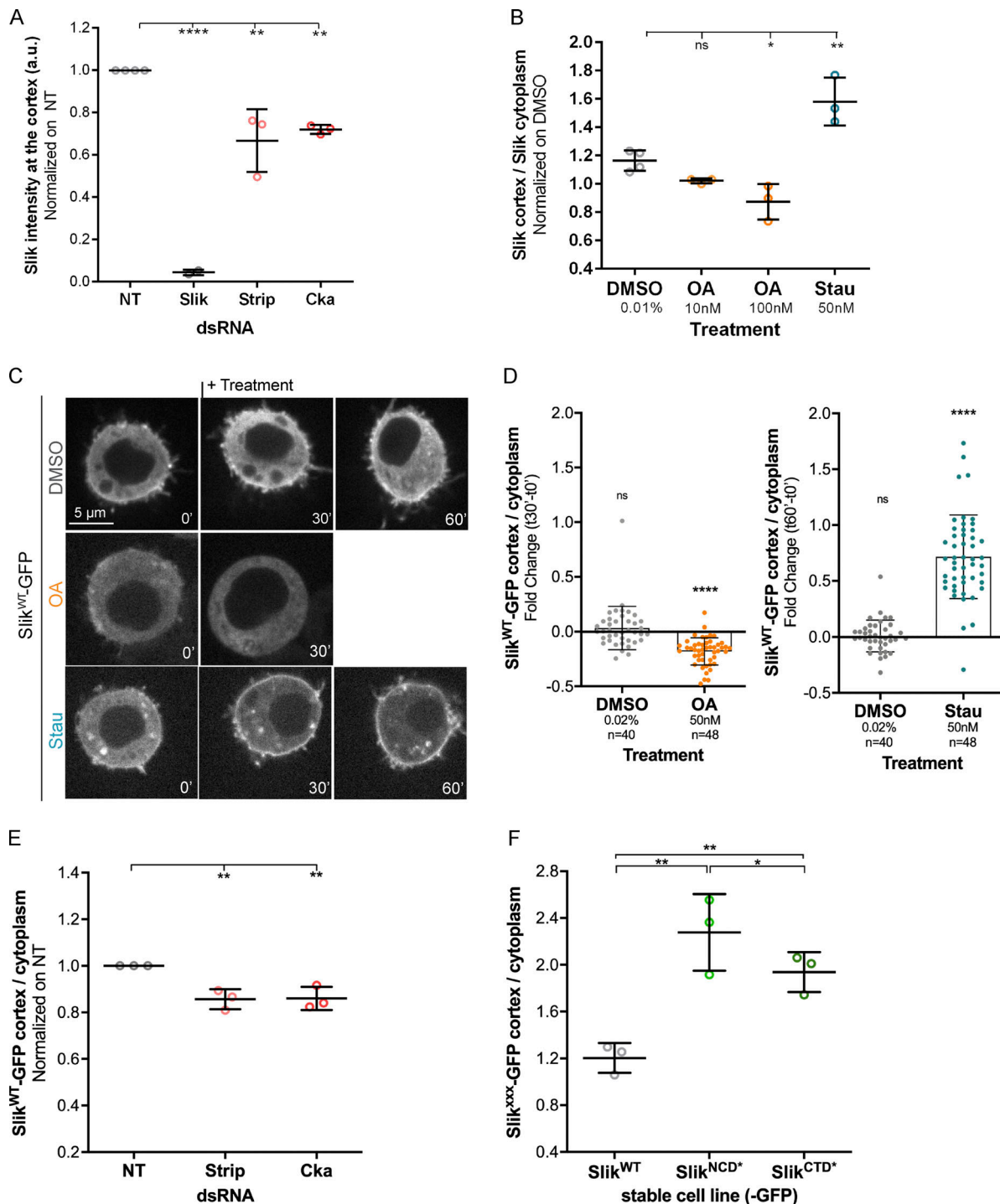
Figure S3. **Slik localization is affected by PP2A$_{STRIPAK}$ inhibition or kinase inhibition. (A)** Slik intensity at the cortex was quantified in a minimum of 60 cells/condition (see Fig. 4 D) in three independent experiments. Data are represented as the mean value ± SD of the pooled replicates (open circles) normalized to the nontarget (NT) dsRNA, one-way ANOVA with the following P values: **, P < 0.01; ****, P < 0.0001. **(B)** The ratio of Slik intensity (cortex/cytoplasm) was quantified in a minimum of 60 cells/condition (see Fig. 4 F) in three independent experiments. Data are represented as the mean value ± SD of the pooled replicates (open circles) normalized to DMSO treatment, one-way ANOVA with the following P values: **, P < 0.01; ****, P < 0.0001. **(C)** Time lapse of Slik distribution in live S2 cell stably expressing Slik^{WT}-GFP (white) upon indicated treatments after the first time frame. **(D)** The ratio of Slik^{WT}-GFP intensity (cortex/cytoplasm) was quantified in a minimum of 12 cells/condition in three independent experiments. Fold changes of the ratio of Slik-GFP before and after the treatments (30 min for OA; 60 min for Stau) were quantified (each dot represents the value for a single cell). Data are represented as mean ± SD of the pooled experiment, paired t test with the following P values: NS, P > 0.05; ****, P < 0.0001. **(E)** The ratio of Slik^{WT}-GFP (cortex/cytoplasm) was quantified in 40 cells/condition (see Fig. 5 B) in three independent experiments. Data are represented as mean ± SD of the pooled replicates (circles), unpaired t test with the following P values: *, P < 0.05; **, P < 0.01. **(F)** The ratio of the indicated Slik-GFP constructs (cortex/cytoplasm) was quantified in 30 cells/condition (see Fig. 5 E) in three independent experiments. Data are represented as mean ± SD of the pooled replicates (circles), one-way ANOVA with the following P values: *, P < 0.05; **, P < 0.01.
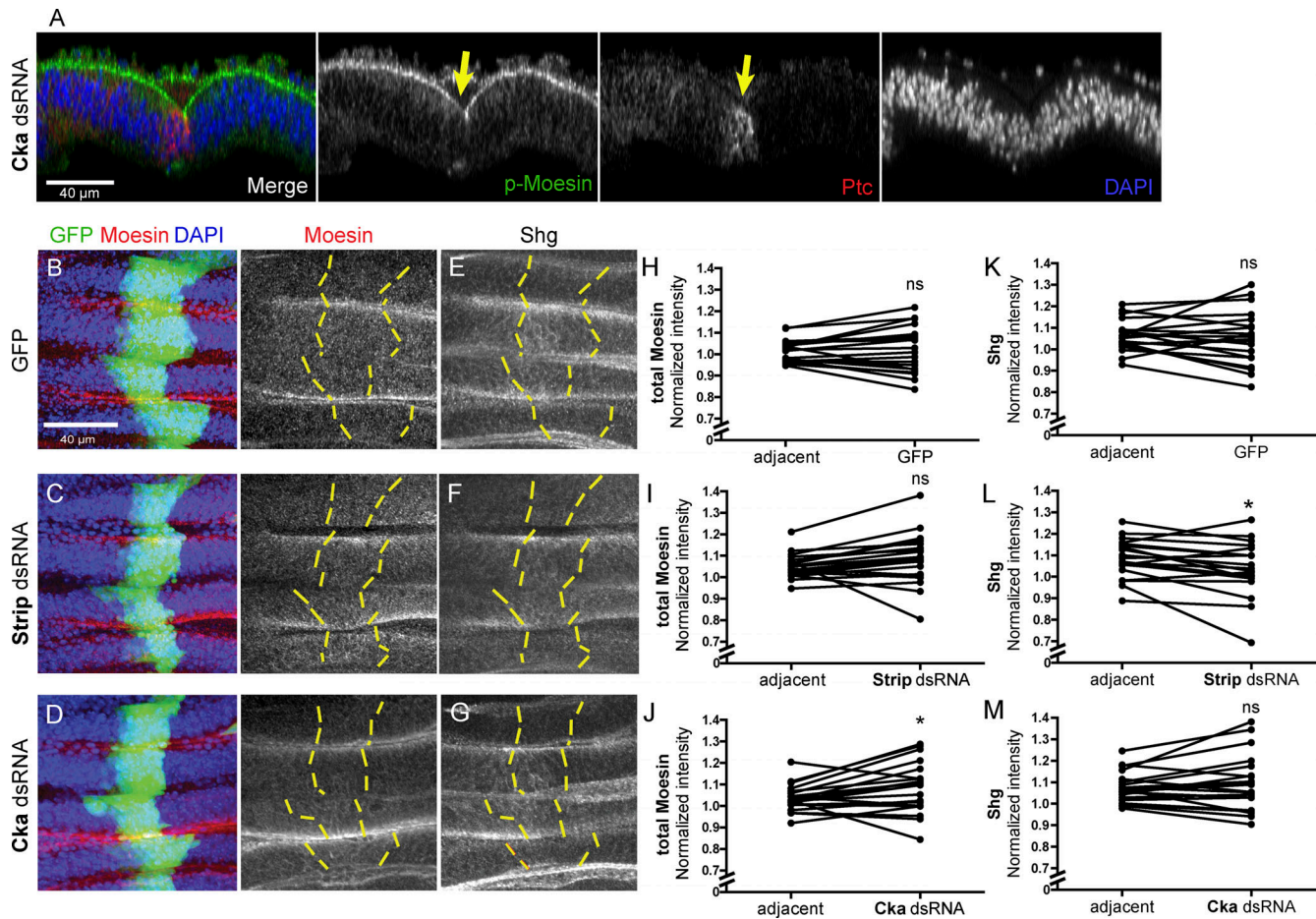
Figure S4. **Strip or Cka depletion has little effect on total moesin and E-cadherin (shotgun) levels and distribution. (A)** X–z section along the anterior–posterior axis of a wing disc expressing P35 together with dsRNA targeting Cka in a central stripe of cells under the control of *ptc*-GAL4. The disc was stained with DAPI (blue) to visualize nuclei and with anti–p-moesin (green) and anti-Ptc (blue) antibodies. The image was generated by orthogonal projection. Apical p-moesin levels are decreased specifically in RNAi-expressing cells in the *ptc* domain. **(B–G)** Confocal projections through medial portions of the hinge region of wing discs expressing GFP (green) in a stripe of cells under control of *ptc*-GAL4, either alone (B and E) or together with dsRNA targeting Strip (C and F) or Cka (D and G). Discs were stained with DAPI (blue) to visualize nuclei and with antibodies against moesin (red) and Shg (shown separately in E–G). Yellow dotted lines indicate limits of the GFP-transgene expression domains. **(H–M)** Quantification of normalized total moesin (H–J) and Shg (K–M) fluorescence intensity in hinge cells expressing GFP alone (H and K) or together with dsRNA targeting Strip (I and L) or Cka (J and M) compared with their respective adjacent wild-type (GFP−) cells. Fluorescence was measured at multiple folds in five wing discs for each genotype. Two-tailed paired sample *t* test with the following P values: NS, P > 0.05; *, P < 0.05. RNAi expression had little effect on moesin and Shg levels and distribution, with only a small increase (4%) in moesin levels in Cka-depleted cells and a small decrease (4%) in Shg levels in Strip-depleted cells. Genotypes: *w,UAS-P35;ptcGAL4/UAS-cka.dsRNA* at 18°C (A); *w;ptcGAL4,UAS-GFP/+* at 25°C (B and E); *w;ptcGAL4,UAS-GFP/UAS-strip.dsRNA* at 25°C (C and F); *w;ptcGAL4,UAS-GFP/UAS-cka.dsRNA* at 25°C (D and G).

Table S1 lists the 51 validated genes from the genome-wide RNAi screen and their activation scores. Data S1 shows lists dsRNA primer sequences. Data S2 shows shows cDNA sequences synthetized for Slik mutants.